The North Sea Light Climate: Analysis of Observations and Numerical Simulations

D. Thewes[1,2*], E.V. Stanev[1,3†], O. Zielinski[4,5‡]

[1]Coastal Research, Institute for Chemistry and Biology of the Marine Environment (ICBM), Carl von Ossietzky University of Oldenburg, Germany
[2]Deutsches Klimarechenzentrum (DKRZ), Institut für Informatik, Universität Hamburg, Hamburg, Deutschland
[3]Institute of Coastal Systems - Analysis and Modeling, Helmholtz-Zentrum Hereon, Geesthacht, Germany
[4]Marine Sensor Systems, Institute for Chemistry and Biology of the Marine Environment (ICBM), Carl von Ossietzky University of Oldenburg, Germany
[5]Marine Perception Research Group, German Research Center for Artificial Intelligence (DFKI), Oldenburg, Germany

Key Points:

- satellite-derived sediment concentration data is fed into a model to study long-term trends in water clarity over the period of 2000-2017.
- Changes in sediment content correspond to changes in water clarity in the model.
- Phytoplankton biomass changes do not directly correspond to changes in water clarity in the model.

*https://orcid.org/0000-0002-6083-8775
†https://orcid.org/0000-0002-1110-8645
‡https://orcid.org/0000-0002-6018-5030

Corresponding author: Daniel Thewes, daniel.thewes@uol.de

Abstract

Recent studies have indicated changes in the light climate of the North Sea. An overall reduction of water clarity over the 20th century could be observed in measurements, and more recent analysis suggests that these trends continue. Inorganic sediment is often named one of the driving factors in these changes and it has been shown to locally increase. With 20 years' worth of satellite-derived sediment data, we were able to conduct basin wide investigations of the temporal dynamics of the biogeochemical state of the North Sea. To identify the impact of inter-annual and seasonal changes in sediment, we fed from two different remote sensing sources (GlobColour & IFREMER) into a 3D coupled hydrodynamic and biological model. The light scheme in the Carbon Silicon Nitrogen Ecosystem model (CoSiNE) was modified to account for sediment specific attenuation. We performed a total of five numerical experiments for the period of 2000 to 2017. The main two experiments were conducted using monthly averaged data. Additionally, as controls, one experiment with annually averaged and one with a 20 year average of sediment, as well as a fifth one without sediment were performed. Our model showed a clear relation between changes in sediment and water clarity. Phytoplankton biomass was reduced only in areas with high nutrient availability.

Plain Language Summary

Studies using satellite or field data have shown that the North Sea has undergone decreases in water clarity and increases in sediment content, while simultaneously showing decreases in phytoplankton biomass over the past century. Declining water clarity would imply inhibited photosynthesis and phytoplankton growth. Phytoplankton itself reduces water clarity. Therefore, the coupling between the three quantities is complex.

In this study, we used satellite-derived sediment data of the years 2000-2017 from two different sources in a three-dimensional model to account for sediment specific effects on underwater light. This way, we were able to determine how changes in sediment content affect water clarity and phytoplankton biomass. The two data sets show different long-term behaviour, with one showing increases and the other decreases. Changes in sediment directly corresponded to trends in water clarity. Long-term changes in the light climate led to changes in biomass in areas of high nutrient availability.

1 Introduction

The light climate in coastal areas is influenced by multiple factors, among them plankton biomass, and dissolved and suspended matter. Although these factors influence each other, they are still independent from each other to a certain degree, as they have different origins. Over the past decades, there have been many successful attempts to model links between phytoplankton growth and other optically active water constituents (e.g. Cahill et al., 2008; Xiu & Chai, 2014; Mobley et al., 2015). However, most attempts are challenging for long-term analysis, due to their immense complexity and computational resource constraints. There may be not enough information about all involved processes and state variables, or the model might be too cumbersome to handle over multi-year computations.

Several studies indicate a decrease in water clarity over the 20th century. These decreases have been linked to colored dissolved organic matter (CDOM) (Dupont & Aksnes, 2013; Opdal et al., 2019) and suspended particulate matter (SPM) (Capuzzo et al., 2015; Wilson & Heath, 2019). It is widely known that bed shear stress is an important control for deposition and resuspension of SPM, and bed shear stress is itself induced mainly by currents and wind waves (Stanev et al., 2009). Wilson & Heath (2019) show that changes in the wind field over the North Sea, English Channel and Irish Sea have led to increased bed shear stress and subsequently to increases in SPM content in several areas. Specifically, with ongoing climate change, strengthened winds have caused

stronger re-suspension of sediments through wind-waves. Wilson & Heath (2019) attribute inter-annual variability in SPM content to variations in bed shear stress. With over 20 years' worth of satellite-derived (non-living) SPM data available, long-term trends within the data are identifiable over large ocean areas. In-situ data is also available for long periods of time, however, the areal coverage is often sparse. It is well known that SPM is one of the major contributors to light attenuation (e.g. Capuzzo et al., 2015; Opdal et al., 2019). This may, of course, lead to the assumption that trends in water clarity would correlate well with trends in SPM. However, due to the insufficient coverage and sparsity of in-situ data, causality remains to be proven.

Darkening of coastal waters may have significant impacts on the entire ecosystem (Capuzzo et al., 2018). Opdal et al. (2019) performed a sensitivity analysis of the effects of non-algal specific attenuation, showing that darkening can lead to belated spring blooms, when the non-algal fraction increases. Schartau et al. (2019) have shown that areas in the North Sea that are rich in total suspended matter (TSM) are associated with inorganic SPM while those that are low in TSM are comparably rich in freshly produced organic SPM. This can be used to classify transition zones from coastal to the outer North Sea, e.g., tidal fronts (Schartau et al., 2019). Significant trends in chlorophyll are not always identifiable over the 20th century (Capuzzo et al., 2015). Some studies even suggest increasing water clarity in some regions in and around the North Sea (e.g. Wiltshire et al., 2008; Gohin et al., 2019). It is obvious that increased light limitation causes inhibited growth. Yet again, it is not clear whether trends in water clarity immediately cause trends in phytoplankton growth, i.e. changes in magnitude or timing.

The seasonality of non-living SPM affects phytoplankton growth, as there is a clear seasonal cycle in SPM concentrations in the North Sea (e.g. Gohin et al., 2005; Stanev et al., 2009; Gohin, 2011; van der Molen et al., 2017). Stronger winds in winter cause increased resuspension of sediments, so that non-living, particularly inorganic SPM typically has seasonal maxima in winter months, which ends when the winds calm in spring. Later in the year, especially where density stratification occurs, sediment concentrations in upper layers are much lower. Phytoplankton undergoes a seasonal cycle as well, which is usually triggered by increasing light availability and temperature in spring. When nutrients become scarce, the spring bloom comes to a halt and is eventually grazed off by zooplankton. The seasonal maxima of non-living SPM and phytoplankton thus do not occur at the same time of the year. For some experiments regarding primary production, these effects might be negligible, but since we focus on long-term changes of non-living SPM, we need to take seasonality into account as to not bias our trend analysis of water clarity.

This study aims to answer, in whole or in part, some of the questions posed by previous works. Specifically, (I) do significant trends exist in the available (satellite-derived) non-living SPM data in the North Sea over the past two decades? (II) Do changes in non-living SPM directly cause changes in water clarity? (III) Is there a noticeable trend in the response of phytoplankton biomass if there are long-term changes in non-living SPM? (IV) Is there a noticeable change in bottom illumination? (V) How do our findings compare to those in literature?

We used a three-dimensional (3D) coupled biological (**C**arb**o**n, **Si**licon and **N**itrogen **E**cosystem model, CoSiNE Chai et al., 2002; Xiu & Chai, 2011) and hydrodynamic (**R**egional **O**cean **M**odelling **S**ystem, ROMS Haidvogel et al., 2000) model and made minor modifications to it, to incorporate offline, satellite-derived non-living SPM as an optically active water constituent. This way, we can simulate attenuation of light due to sediment over a multi-year period. We bypassed the need to set up a sediment and wind wave model alongside ROMS-CoSiNE, which makes the model more cost efficient than the alternative. The usage of offline, satellite-derived data enables us to analyze the impact of observed changes in non-living SPM on the North Sea ecosystem. The method is similar to that used e.g. by Wakelin et al. (2012) and Wakelin et al. (2015), who made use of satellite products to account for non-biotic light attenuation, however, they did not spec-

ify between CDOM- and SPM-specific attenuation. Instead of on light climate, their work focussed on modelling carbon fluxes of the north eastern Atlantic and the European shelf.

We performed several numerical experiments, utilising two different sources of non-living SPM, to investigate the mechanistical link between sediment, water clarity and biomass, over a time period of 20 years from the 1st of January 1998 to 31st of December 2017, using the first two years as spin-up. As a measure for water clarity, we calculated the 1%- and 10%-depths (z_1 and z_{10}, respectively) at all horizontal grid points for every day in the entire period. The days at which z_1 was not defined, i.e. bottom irradiance was above 1% of the surface value, are defined as bottom illumination days N_d. Note that due to the assumption that SPM was distributed vertically homogeneous, N_d as derived from the model is not to be understood as equivalent to a related quantity that was measured in-situ (see section 4.2 for details). Linear regression analysis was performed on z_{10}, as well as the satellite-derived SPM data (averaged monthly and interpolated onto our $7km \times 7km$ grid), the depth integrated phytoplankton biomass above z_{10}, and N_d.

2 Methods

2.1 The Physical Model

The hydrodynamic model we used is ROMS. A full description of the general set-up can be found in Thewes et al. (2020). The lateral domain extends from $5°W$ to $13°E$ and $48°N$ to $60°N$ with a resolution of $7km$. The vertical domain is divided into 35 s-layers (Song & Haidvogel, 1994), stretched to increase the resolution at the surface. Vertical turbulence closure was achieved by utilising the generic length scale (GLS) approach in a k-kl configuration (Umlauf & Burchard, 2003; Warner et al., 2005). Figure 1a shows the model bathymetry. The horizontal grid is taken from the Atlantic Margin Model at $7km \times 7km$ resolution (AMM7 O'Dea et al., 2012, 2017). It ranges from $4.5°W$ to $13°E$ and from $48°N$ to $59.5°N$.

The initial and boundary conditions (IC and BC) were also taken from AMM7. We utilised a Chapman type BC for daily means of sea surface height (SSH), superposed with tidal forcing from the finite element solution model (FES, the 2014 model as provided by AVISO). The two-dimensional (2D) momentum BC was introduced via a Schchepetkin BC (Mason et al., 2010). Temperature, salinity, nutrients (see 2.2) and 3D momentum are introduced via a radiation BC with nudging (Orlanski, 1976; Marchesiello et al., 2001). The atmospheric BC was taken from NCEP/NCAR and is of quarter daily and $21km$ lateral resolution. The river input is climatological daily means, taken from the pan-European Hydrological Predictions for the Environment (E-HYPE) model of the Swedish Meteorological and Hydrological Institute (SMHI).

2.2 The Biological Model

The biological model that was used is the CoSiNE model, developed by Chai et al. (2002) and further developed by Xiu & Chai (2011). In the version we used, it consists of 11 state variables: four nutrients (NO3, NH4, SiOH4 and PO4), four plankton groups (small phytoplankton (P1), diatoms (P2), microzooplankton (Z1) and mesozooplankton (Z2)), detrital nitrogen (dN) and silicate (dS), as well as oxygen. The details and equations are found in Chai et al. (2002) and Liu et al. (2018). The biological BC and IC are taken from AMM7, coupled to the European Regional Sea Ecosystem Model (ERSEM Baretta et al., 1995; Blackford et al., 2004). The nutrients are introduced via a radiation BC with nudging. Plankton and detritus were treated via a radiation BC without external nudging (Orlanski, 1976; Marchesiello et al., 2001). Riverine nutrients are taken from E-HYPE. The variables that are unavailable either at the open boundaries or at rivers are assumed by using typical ratios, e.g., NH4 is assumed to be a tenth of the amount of NO3. All model parameters are listed in table A1.

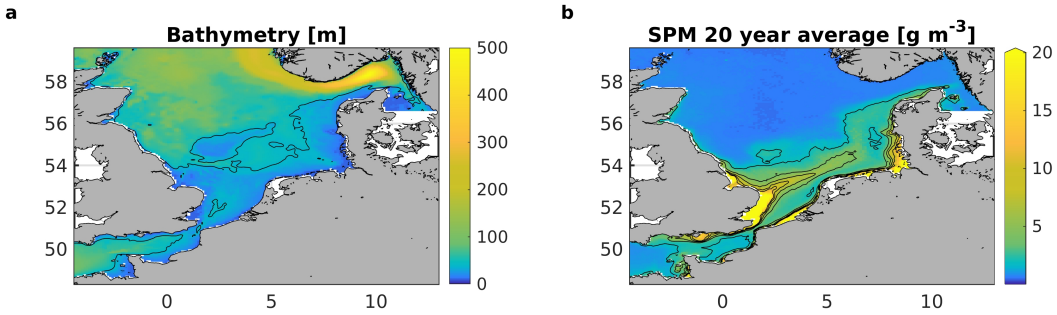

Figure 1. a: model Bathymetry. The black isoline denotes the $40m$-isobath. b: 20-year average of IFREMER (non-living) SPM as it is fed into IF20Y. Contour intervals are at 2, 4, 6, 8 and $10gm^{-3}$. Note that the color map is saturated above $20gm^{-3}$. White areas in both panels are outside of the model grid.

2.3 Incorporating Sediment

Note that going forward, whenever we write 'SPM', we refer only to the non-living fraction. We use SPM data obtained from satellite imaging and provided by IFREMER (IFREMER, 2017), as well as data from GlobColour (`http://globcolour.info`). Both data sets were generated using the algorithm defined by Gohin et al. (2005) and Gohin (2011), known as OC-5. The original algorithm was designed for case 1 waters (Gohin et al., 2005). SPM is calculated using water leaving radiance nLw, which, after atmospheric correction, is the quantity provided by the sensor. The sensors employed in the respective datasets are SeaWIFS, MODIS/AQUA and MERIS for IFREMER, merged following Saulquin et al. (2011), and for GlobColour, the same as for IFREMER, and additionally, VIIRS NPP, VIIRS JPSS-1 and OLCI-A. The GlobColour data was merged via weighted averaging (see IOCCG Report Number 4, 2004). nLw is linearly related to reflectance R^*. Data pairs of chlorophyll-a and non-living SPM from in situ measurements are used to obtain R^*. With theoretical estimates of absorption a and backscatter b_b, corresponding to said data pairs, R^* is regressed at $555nm$ via the relation

$$R^*(555) = \alpha_0 + \alpha_1 nLw(555) = \frac{b_b(555)}{a(555) + b_b(555)}. \tag{1}$$

The relation between R^* and $nLw(555)$ is then inverted to optain SPM, yielding

$$SPM = \frac{R^*(555)\,[a_w + a_{P+Y}(CHL)] - [b_{b,w} + b_{b,CHL}(CHL)]}{b^*_{b,SPM} - a^*_{SPM} R^*(555)}, \tag{2}$$

where a_w, a_{P+Y} and a^*_{SPM} are the absorption coefficients specific to pure water, chlorophyll-a and yellow substances (i.e. CDOM), and sediment, respectively. $b_{b,w}$, $b_{b,CHL}$ and $b^*_{b,SPM}$ are the backscatter coefficients for pure water, chlorophyll-a and sediment, again, respectively. The absorption by yellow substances can be neglected under the assumption that they do not contribute to absorption at wavelengths larger than 550nm. Phytoplankton specific absorption and backscatter are known, having been measured with the same sensor.

The algorithm tended to underestimate SPM in turbid near shore waters, which is why it was refined in Gohin (2011) to include a second channel at $661nm$ wavelength. If for both wavelengths ($555nm$ and $661nm$), SPM is lower than $4gm^{-3}$, the $555nm$-channel is conserved. Otherwise, SPM is taken from the $661nm$-channel. The algorithm was calibrated between $0.5gm^{-3}$ and $40gm^{-3}$. For higher values, saturation may occur.

The data are provided as daily means, which are averaged monthly. Due to cloud coverage, there may be data gaps for sometimes longer than a week. For this reason, the

monthly means consist of a variant number of data points. However, this number is particularly low in winter months, when there is little to no primary production, hence the error in the bio-model is negligible.

The monthly SPM means are then interpolated bilinearly onto the model grid, and read into ROMS as a 2D-array, where it is treated in a similar fashion as for instance atmospheric forcing is, i.e. it is interpolated linearly in time between two time frames, to match the current model time. The 20-year average of SPM from 1998-2017 is displayed in figure 1b.

The measured SPM is defined as above the penetration depth. Therefore, we have no information about the SPM concentration near the bottom. However, we assume the portion of SPM most important to light attenuation to be mainly in the upper water column and approximately vertically homogeneous. Consequently, we assume the distribution of SPM to be constant throughout the entire water column. Given that SPM tends to accumulate at the bottom of a water column, we thus likely underestimate SPM specific attenuation below the photic depth, and particularly in the $5-10m$ above the bed. In shallow coastal waters with high sediment content, such as in the southern North Sea, the water column is only weakly, if at all, thermally stratified. Generally speaking, the North Sea can be assumed to be thermally stratified only in deeper regions and only at times where there is little wind induced mixing, i.e. in summer, where there is generally low phytoplankton growth due to nutrient limitation. Thus we assume the water column is well mixed when SPM content is highest. We admit that this need not be the case at all times. Furthermore, there is no sound method to extrapolate SPM downwards without adding additional uncertainty.

The equation for irradiance with depth is then

$$I(z) = I_0 \exp(-k_w z - \int_z^\zeta k_P(P1(z') + P2(z'))\mathrm{d}z' - k_{SPM} SPM \cdot z), \tag{3}$$

where k_w, k_P and k_{SPM} are the respective attenuation coefficients for pure water, phytoplankton and SPM, and I_0 is the surface level irradiance. The individual contributions to attenuation in the exponential of equation 3 will forthgoing be denoted by a capital letter K, e.g., $K_P = \int_z^\zeta k_P(P1(z') + P2(z'))\mathrm{d}z'$.

2.4 Experiment Design

We computed 20-year simulations from 1998 to 2017, using the years 1998 and 1999 as spin-up. A total of 5 different long-term runs with different SPM configurations were performed: a control run without SPM (NOSPM), two runs using monthly means, once of GlobColour (GCMON) and once of IFREMER data (IFMON), and two more using IFREMER data, but with annual (IFANN) or 20-year averages (IF20Y). Here, IF20Y, like NOSPM serves as a negative control.

2.5 Methods of Analysis

To have quantities that are directly related to water clarity, we computed z_1 and z_{10} for every horizontal grid point and every time step. Both are defined positive upwards and are thus always negative. Lower magnitudes mean lower water clarity. It is obvious that z_1 or z_{10} cannot be calculated if bottom irradiance in the model is above 1% or 10% of surface irradiance, respectively. Therefore, z_{10} is more often available than z_1, which makes it a more reliable measure for water clarity. To calculate N_d, we counted the days within a year during which the average modelled bottom irradiance was larger than 1%. To quantify the biomass that is affecting z_{10}, we integrated the phytoplankton biomass over depth from z_{10} to the surface ζ, i.e.

$$P1_{10} = \int_{z_{10}}^\zeta P1\mathrm{d}z, \tag{4}$$

and accordingly for $P2$. The total biomass above z_{10} will be denoted as $P_{10} = P1_{10} + P2_{10}$. Note also that the total biomass above z_1 is only marginally larger than P_{10}.

For validation purposes, we make use of in situ chlorophyll data, provided by the International Council for the Exploration of the Sea (ICES). To compare our model results to the data, we interpolated P_{10} and z_{10} bilinearly between the four nearest grid points to a singular data point, and divide them by each other to obtain the vertically averaged nitrogenous phytoplankton biomass above z_{10},

$$\tilde{P}_{10} = P_{10}/z_{10}. \tag{5}$$

We performed linear regression analysis on z_{10}, P_{10}, N_d and the input SPM data to quantify trends in water clarity (note that when we write SPM, italic, we refer to the input data specifically and otherwise to SPM in general). To increase the goodness of the fit, we perform the regression on annual means of the respective variables. This way, we remove seasonal variability, which does not affect long-term trends. However, because the SPM data's error margins are particularly high in winter months, due to cloud coverage, yet, there is no significant phytoplankton growth during this time, we also performed the regression analysis on March to September means for z_{10}, P_{10} and SPM. For a more detailed discussion on this method, see section 4.2. For all regression models, we calculated the goodness of fit (also known as the coefficient of determination)

$$R^2 = 1 - \frac{\sum_t^{N_t}(x_t - \tilde{x}_t)^2}{\sum_t^{N_t}(x_t - \mu_x)^2}, \tag{6}$$

where x_t is the model output for phytoplankton, or the model input of SPM, $\tilde{x}_t = at + b$ is the linear regression model with a being the slope and b being the y-intercept, and μ_x being the long-term mean of a variable x over the period of N_t days. To further determine statistical significance of the linear regression, we perform a t-test, where the null-hypothesis is that there is no linear relationship between t and x_t, i.e. $R^2 = 0$. If the probability p of the null-hypothesis being true is less then 5%, it is rejected, i.e. the linear trend is significant.

3 Results

3.1 Comparison between satellite and in-situ *SPM*

To demonstrate the validity of the data sets used in this study, we compare both to in-situ data, provided by Rijkswaterstaat (Netherlands, locations in figure 2a, names and coordinates in tab. 1). Note that the in-situ data is actually TSM, i.e., containing organic SPM. For this reason, we apply a method described by Schartau et al. (2019, their eqn. 10, table 2, seasonal fit), to obtain the organic fraction as a function of TSM, to inversely compute inorganic SPM. Linear regression of satellite-derived SPM as a function of in-situ data yields

$$SPM_{IFREMER} = (-0.006 \pm 0.043)mg^{-3} + (0.908 \pm 0.017)\cdot SPM_{in-situ} \tag{7}$$

and

$$SPM_{GlobColour} = (-0.013 \pm 0.021)mg^{-3} + (0.743 \pm 0.014)\cdot SPM_{in-situ}. \tag{8}$$

As this comparison shows, the satellite products tend to underestimate SPM, GlobColour data more so than that of IFREMER. This is partially explained by the nature of the products compared. While an in-situ measurement is an instantaneous sample at a very specific point in time, a single pixel of a satellite image is in orders of square kilometers in size and often averaged from multiple images per day. Thus, in-situ measurements tend to be scattered much more strongly and may reach higher magnitudes. Note also that the in-situ data was not necessarily collected using the method described by Röttgers et al. (2014) and was not corrected accordingly, and therefore is likely biased positively. Lastly, the conversion from TSM to SPM following Schartau et al. (2019) is empirical and therefore inherently error prone.

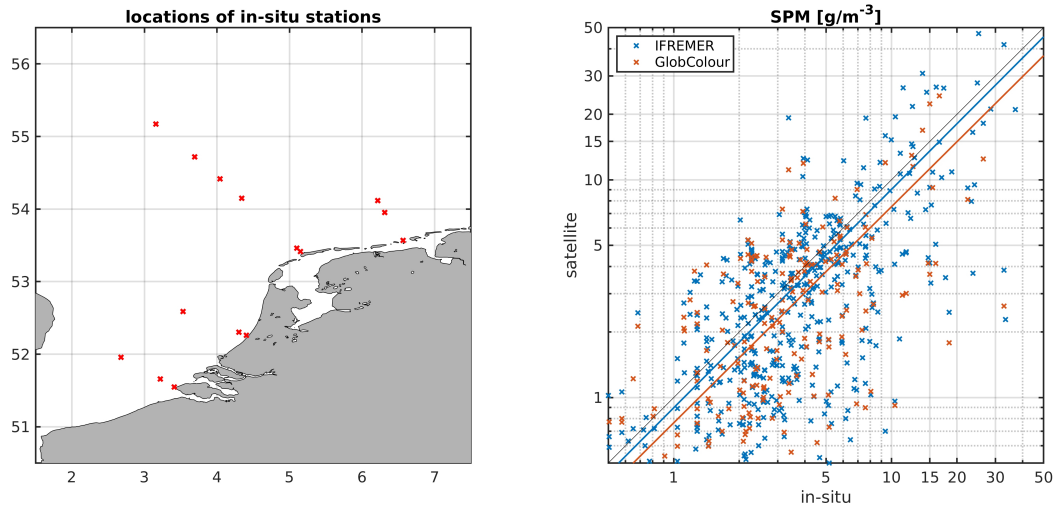

Figure 2. a: Locations of all used in-situ stations. b: Comparison of satellite vs. in-situ SPM for IFREMER (blue) and GlobColour (red).

Table 1. Names and coordinates of in-situ stations for SPM comparison against satellite products.

Name	Longitude [$°E$]	Latitude [$°N$]
Noordwijk 2km offshore	4.4061	52.2614
Noordwijk 10km offshore	4.3025	52.3022
Noordwijk 70km offshore	3.5314	52.5861
Rottumerplaat 3km offshore	6.5642	53.5661
Rottumerplaat 50km offshore	6.31	53.9539
Rottumerplaat 70km offshore	6.2142	54.1181
Terschelling 4km offshore	5.1506	53.4153
Terschelling 10km offshore	5.1008	53.4611
Terschelling 100km offshore	4.3419	54.1494
Terschelling 135km offshore	4.0411	54.4156
Terschelling 175km offshore	3.6917	54.7192
Terschelling 235km offshore	3.1575	55.1722
Walcheren 2km offshore	3.4108	51.5489
Walcheren 20km offshore	3.2206	51.6586
Walcheren 70km offshore	2.6792	51.9569

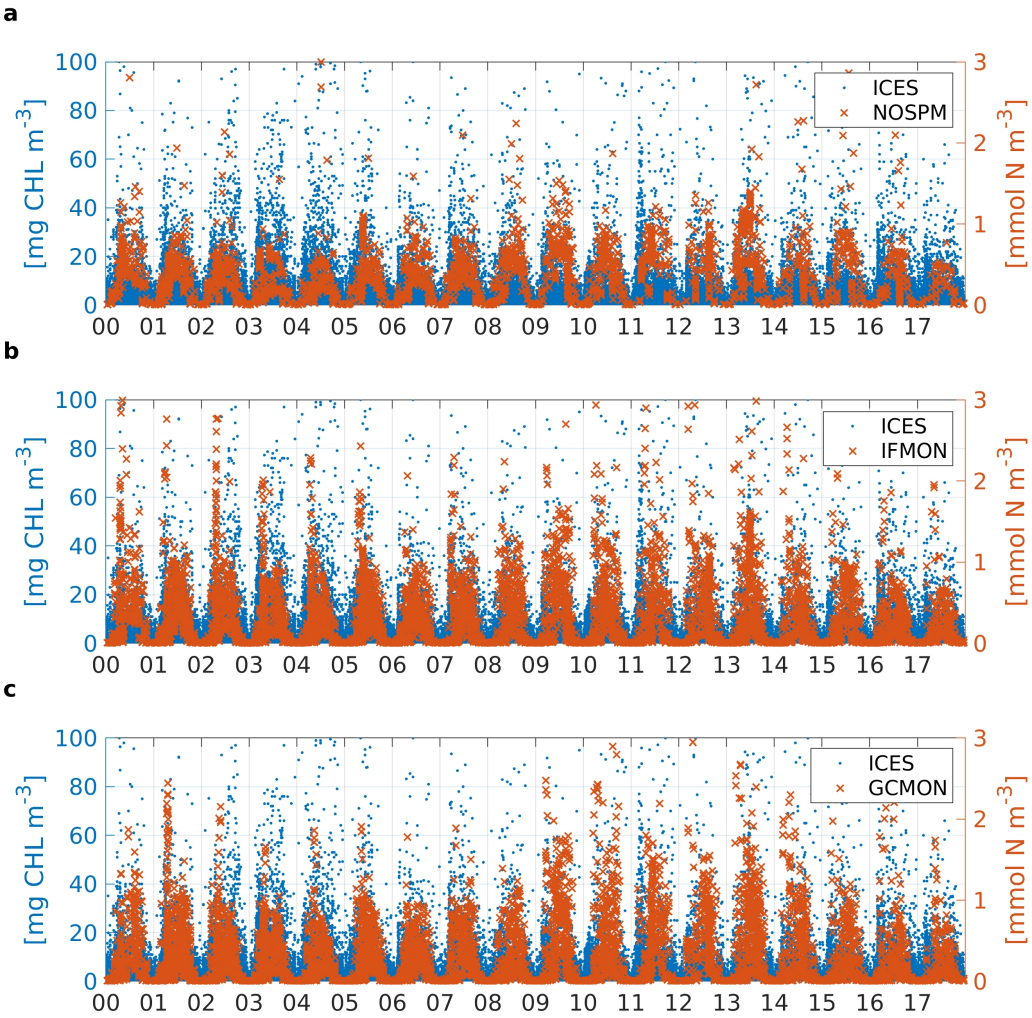

Figure 3. in-situ chlorophyll bottle data from ICES (blue axis) and $\tilde{P}_{10}$ (red axis) over the period of 2000-2017 for NOSPM (a), IFMON (b) and GCMON (c).

3.2 Comparison between model and in-situ data

Our model is capable of simulating the seasonal plankton dynamics of the North Sea. A comparison to in situ bottle data of chlorophyll from ICES reveals that the model reproduces the chlorophyll cycle reasonably well, as is shown for NOSPM, as well as for IFMON and GCMON in figure 3. Note that we are comparing chlorophyll data to nitrogenous biomass, so the ranges of magnitude do not match. However, the peak to crest relations are very similar for the in-situ chlorophyll data, compared to the models.

3.3 Effects of SPM on attenuation

The effect of SPM on attenuation is visualized in figure 4, which in panel b shows vertical profiles of irradiance, normalized to the surface level for NOSPM and IFMON. Specifically, these profiles are taken from a station at the Oyster grounds ($4.33°E$ and $53.43°N$, marked by a red cross in figure 4a) at times t_1 (31^{st} of January 2000, as a typical winter situation) and t_2 (1^{st} of May 2000, the spring bloom peak day in NOSPM), and t_3 (14^{th} of May 2000, the spring bloom peak day in IFMON). Note that the irra-

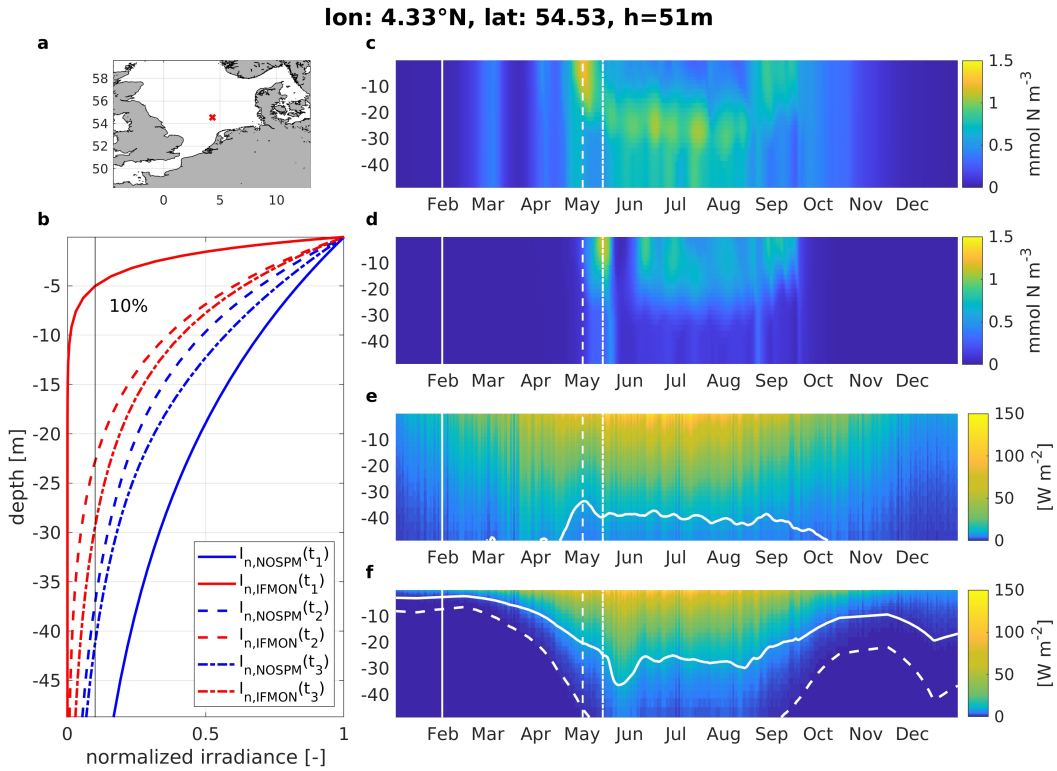

Figure 4. a: location of the shown station within the North Sea. b: normalized irradiance for NOSPM (blue) and IFMON (red) at times t_1, t_2 and t_3 (31st of January, 1st of May and 14th of May 2000), respectively. c and e: phytoplankton biomass [$mmolNm^{-3}$] for NOSPM (c) and IFMON (e) in the year 2000. d and f: normalized irradiance for NOSPM (d) and IFMON (f). Solid white line in d and f denotes z_{10} and dashed white line in f denotes z_1. The vertical lines in c-f denote t_1 (solid), t_2 (dashed) and t_3 (dotted dashed).

diance profiles for IFMON all decay significantly faster with depth than those in NOSPM. Particularly in the winter situation at t_1, NOSPM decays the slowest of all three example times, while IFMON decays the fastest.

The right-hand panels (c-f) show phytoplankton biomass (c and d) and irradiance at depth (e and f) for the two runs over the year 2000. SPM influence furthermore causes a slight delay in spring bloom peak time, as can be seen in figure 4c and d. The inclusion of SPM leads to shallower z_1 and z_{10}, as it is to be expected (figure 4e & f, dashed and solid white contour lines, respectively). In fact, there is no occurrence of z_1 at this station at any time for NOSPM. It becomes clear that SPM strongly reduces light availability, but mostly so in winter months. It is also apparent from figure 4c and d that NOSPM exhibits several small, early phytoplankton blooms before the onset of the actual spring bloom, peaking at t_2. These are completely suppressed in IFMON. The period of primary production in IFMON also ends earlier than in NOSPM by almost two months.

Figure 5 shows the individual contributions of SPM and phytoplankton to attenuation (see section 2.3) for IFMON (panels a & c) and GCMON (b & d). The contribution of phytoplankton is an order of magnitude lower than that of SPM. Note that in GCMON, K_{SPM} peaks higher and the trail of the peak prolongs well into June (b), while in IFMON, there is a much faster decline in K_{SPM} (a). Accordingly, K_P peaks later in GCMON by about two weeks, relative to IFMON, yet more strongly. For the months July to September, K_P is almost identical between the two runs. Figure 5e shows

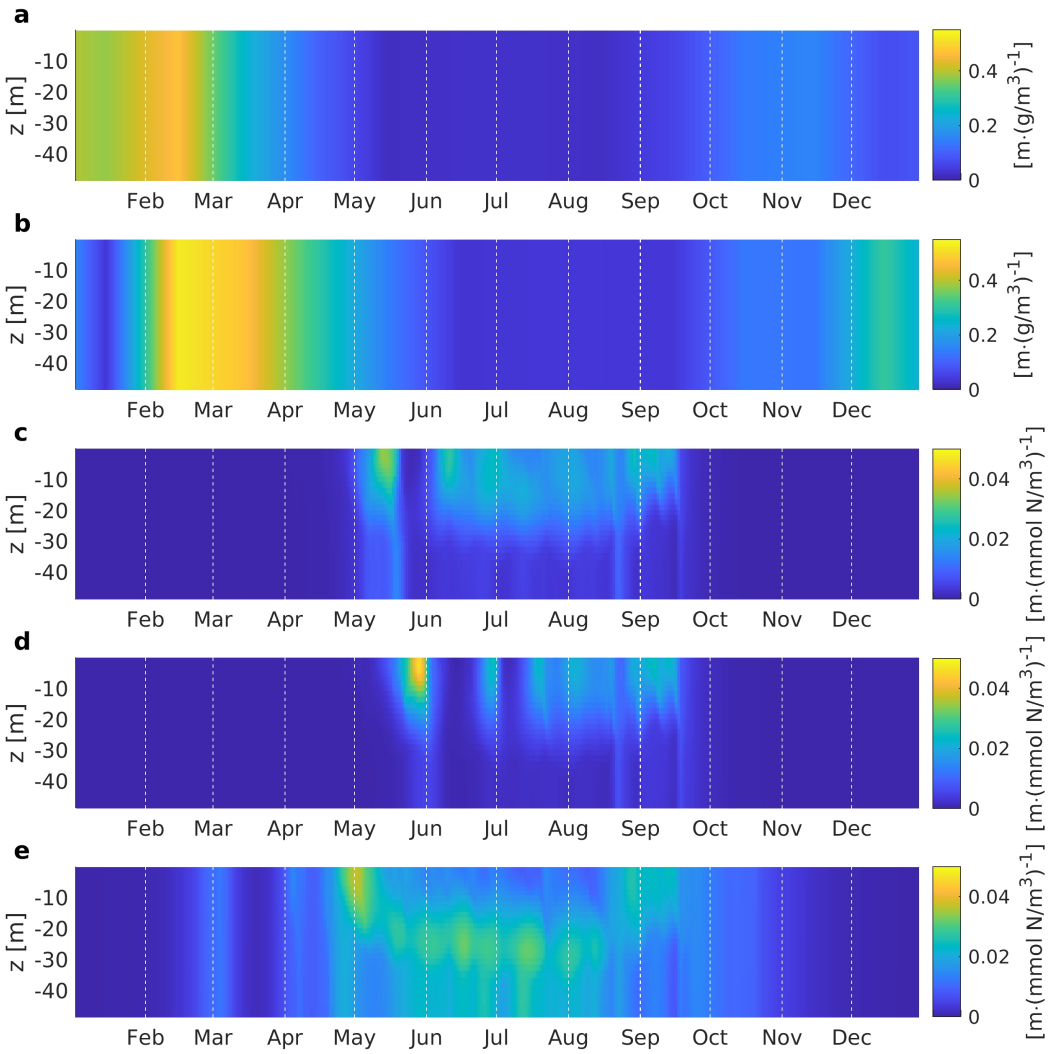

Figure 5. K_{SPM} (a & b) and K_P (c & d) for IFMON (a & c) and GCMON (b & d), and K_P for NOSPM (e) for the year 2000 at the position marked by the red cross in figure 4a.

the contribution of phytoplankton to attenuation in NOSPM, which is, absent of SPM, is the only contributor. Unlike the other runs, the earliest bloom occurs in March. The September bloom is of slightly higher magnitude, and it prolongs until November, but otherwise, it is similar to that of IFMON and GCMON. Noteworthy is also that in NOSPM, the phytoplankton maximum is consistently at mid water column.

To gain an understanding of horizontal patterns, figure 6 shows long-term means of z_{10} for 2000-2017. On average, z_{10} in IFMON is about 33% of that in NOSPM. The other SPM runs show similar reductions, pattern wise, but larger in magnitude, with average z_{10} of 30% of NOSPM's z_{10} (not shown). The differences in z_{10} between the SPM runs are most pronounced in shallow regions with large variability in SPM, where IFMON's z_{10} is about 10% deeper than in IFANN or IF20Y. For large areas in NOSPM, the bottom irradiance is above 10% of the surface level at all times. This is nowhere the case in any of the SPM runs.

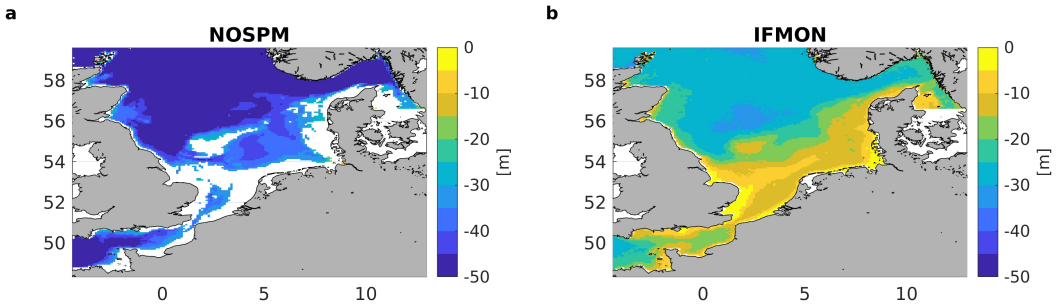

Figure 6. Long-term average of z_{10} over 2000-2017 for NOSPM (a) and IFMON (b). Blank areas are grid points at which the bottom layer irradiance is higher than 10% of the surface irradiance at all times.

3.4 Long-term trends

The results of the linear regression of SPM for averages over the spring and summer show differences between the input data sets. As figure 7 shows, the areas where the trends are found to be significant ($p < 0.05$) rarely overlap, yet when they do, the slopes typically have the same sign (e.g. north of Norfolk, England, or in small regions along the french coast). Opposing signs in the slopes of SPM are nowhere to be found in regions where $p < 0.05$ for both runs. The only strong disagreement is found at the Thames plume, $52°N$ and $2°E$, where IFREMER shows strong increases and GlobColour strong decreases in SPM, yet, in both cases, with low R^2. Overall, trends in GlobColour are more negative (decreasing SPM) than in IFREMER, where the significant trends tend to be positive (increasing SPM). The analysis over annual means show disagreement in overlapping regions (see figure B4), suggesting that data uncertainties in winter cause spurious trends (see sec. 4.2 for details).

The slopes and R^2 of the regression of z_{10} are shown in figure 8. At first glance, it is obvious that for many regions where there is a significant trend in SPM (demarked by the red contour line), there is also a significant trend in z_{10}, which is true for both data sets. Accordingly, the slopes in z_{10} tend to differ between the two runs. This is particularly the case above $55°N$, where IFMON shows predominantly positive slopes, i.e. a shallowing of z_{10} (a negative quantity), and GCMON shows a deepening. In several areas, the slopes overlap and where they do, they are of the same sign and often comparable magnitude (grey ellipses in figure 8). Opposing trends are hardly ever significant ($p < 0.05$) in both IFMON and GCMON. Note also that in the region south of the Dogger Bank (around $54°N$ and approximately between $2°E$ and $4°E$), the GCMON run shows a shallowing of z_{10}, while there is no significant trend in GlobColour SPM there. There is, however, a similar shallowing trend in z_{10} in IFMON. Also note that there are exceptions from the rule that z_{10} slopes tend to follow SPM slopes. It stands to be noted that the two data sets - while exhibiting differences - do not fundamentally contradict each other when applying the regression analysis only on spring and summer. See figure B4 in the supplemental material to see the results of the analysis on annual means, which do contradict each other.

By division of the regression slopes of z_{10} by the 20-year averaged SPM for the months March to September, we obtain relative changes, which are displayed in figure 9. Note that the relative change refers to the magnitude, i.e. the absolute of z_{10}. Thus, a negative relative change means a shallowing and a positive change means a deepening of z_{10}. The two runs, IFMON and GCMON, share several similarities, but GCMON seems to be shifted positively relative to IFMON by $0.01 - 0.03$, non-uniformly. GCMON shows predominantly deepening trends, while IFMON shows more shallowing trends. The shallowing in IFMON is most pronounced in the English Channel, which is also the

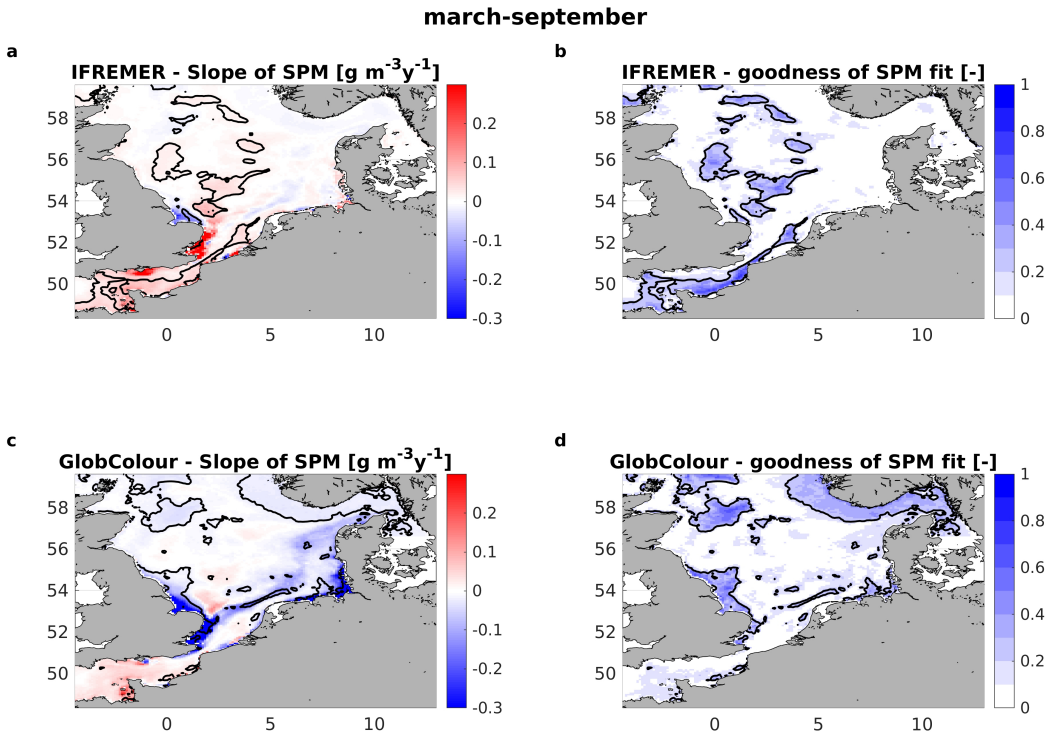

Figure 7. Linear regression slopes (a&c) and R^2 (b&d) for IFREMER (top row) and GlobColour (bottom) SPM data, averaged over spring and summer. Black contours demark the $p = 0.05$ significance threshold for linear regressions of SPM.

region from which the calibration of the IFREMER data set was taken (Gohin, 2011).

The changes in P_{10} (March to September) are shown in figure 10. It is obvious that changes in GCMON are almost entirely negligible (figure 10c). The inclusion of SPM does not appear to play a role there. On the other hand, IFMON shows very clear decreases in the southern North Sea and in the English Channel, which are aligned with increases in SPM (compare figure 7 and red contour in figure 10a&b). This indicates that decreases in SPM seem to affect P_{10} less than increases.

Looking at the average annual number of days with bottom illumination N_d is helpful to illustrate crucial differences between the five experiments (figure 11). IFMON and GCMON look very alike, with only minor differences. However, IFANN shows several notable differences to the former two, in that there are significantly lower values of N_d ($< 50d$) along most of the coasts, while some areas (e.g. near the mouth of the Rhine, at $\approx 53°N$ and $\approx 4.5°E$) show values above $> 300d$. Also, the Dogger Bank (around $55°N$ and between $1°E$ and $5°E$) shows higher numbers of N_d as well. There is a tendency for values of $N_d \gtrapprox 200$ in IFMON or GCMON, the corresponding value in IFANN is higher, and lower for $N_d \lessapprox 200$, respectively. This is even more so the case for IF20Y, where the same general behaviour can be observed, but there is hardly any middle ground between $N_d > 300$ and $N_d < 30$. Lastly, the NOSPM experiment shows entirely unrealistic values of N_d. Here, all areas that are shallower than 100m are fully illuminated throughout the entire year. This emphasizes the necessity of seasonality in SPM, particularly when considering benthic dynamics.

The long-term changes of N_d are shown for IFMON and GCMON in figure 12, for months March to May and June to August. From March to May, the two runs show rather little agreement, although showing little overlap or contradiction. This, again, hints to

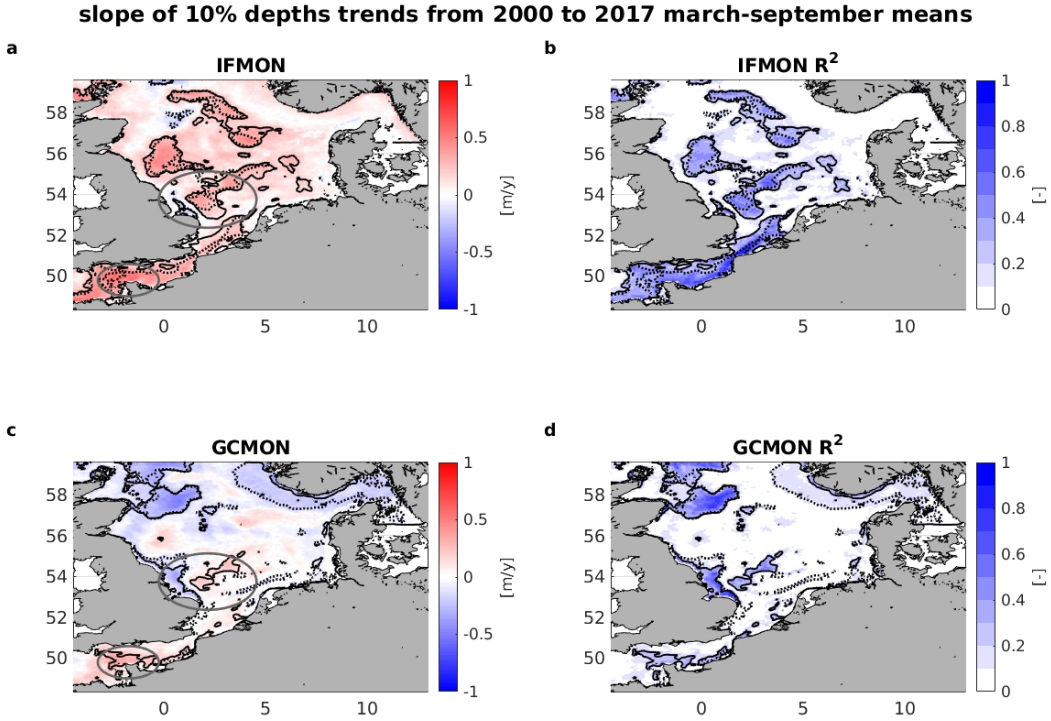

Figure 8. Slopes (a&c) and R^2 (b&d) of z_{10} for IFMON (top row) and GCMON (bottom row). Dotted black demark the $p = 0.05$ contour line of the respective SPM data set's linear regression slopes (compare figure 7). Solid black contours demark the $p = 0.05$ significance threshold for linear regressions of z_{10}. Grey ellipses mark areas of significant trends overlapping between the two data sets.

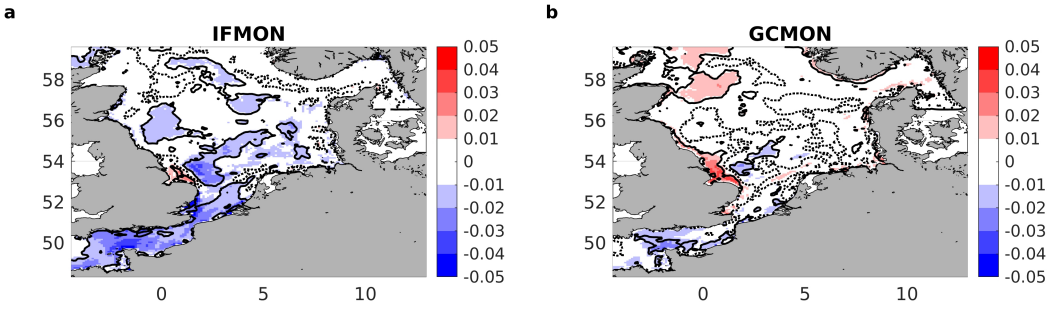

Figure 9. Slopes of z_{10} for IFMON (left) and GCMON (right), relative to the 20-year averaged z_{10} means from March to September. Solid black contours demark the $p = 0.05$ contour line of the respective z_{10} linear regression slopes (compare figure 8). Dashed black contours demark 0.

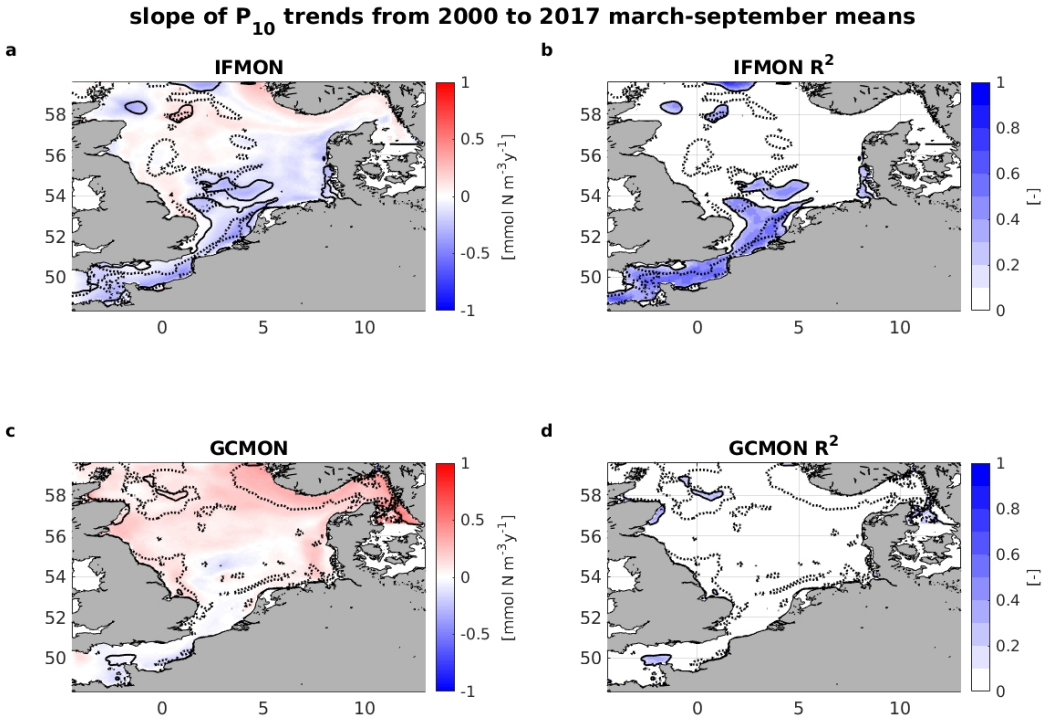

Figure 10. Slopes (a&c) and R^2 (b&d) of P_{10} for IFMON (top row) and GCMON (bottom row). Dotted contours demark the $p = 0.05$ contour line of the respective SPM data set's linear regression slopes (compare figure 7). Solid black contours demark the $p = 0.05$ significance threshold for linear regressions of z_{10}.

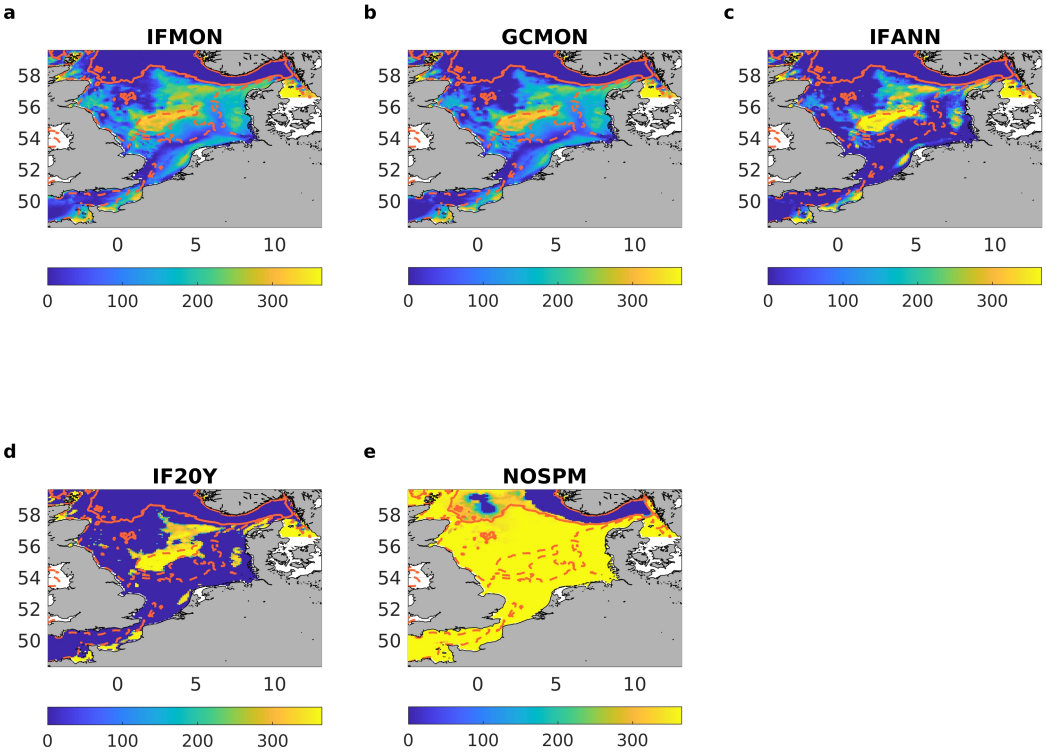

Figure 11. N_d for IFMON (a), GCMON (b), IFANN (c), IF20Y(d) and NOSPM(e). The red contour lines denote isobaths, specifically $40m$ (dashed) and $100m$ (solid).

a potential bias between the long-term trends of the two runs, like for SPM or z_{10} (figure 7 & 9). However, for the summer months, there are many regions of agreement, particularly west of $4°W$, where both GCMON and IFMON show decreases of N_d, except along the eastern shore of England and Scotland, north of $53°N$. IFMON shows weaker increases and stronger decreases in N_d than GCMON, which also hints at the previously implied bias. Still, particularly in the area from $51°N$ to $55°N$ and $0°$ to $3°E$, the magnitudes match well. Note that a change of $5dy^{-1}$ corresponds to a decrease of $100d$ over twenty years. However, the seasons are only about $90d$ long, so in essence, the regions where there are changes of $\approx \pm 5dy^{-1}$, the region changes from completely light to completely dark, or the inverse, respectively. Discussion on the applicability of linear regression is found in section 4.2.

4 Discussion

4.1 Addressing the Research Questions

In section 1, several research questions were introduced. The first (I) was whether significant trends existed in the available (satellite-derived, non-algal) SPM data in the North Sea over the past two decades. Indeed, using the method of linear regression, we found that there were several areas showing a significant long-term change in SPM. However, the two data sets hardly showed any overlap in those areas. As previously mentioned, this might indicate a drift, i.e., a bias in the long-term trend in either data set, relative to the others. Focussing only on spring and summer, those trends that were found were rarely much more than moderately significant ($0.4 < R^2 < 0.6$). The IFREMER data showed increases in SPM along the southern shore of the English Channel and North

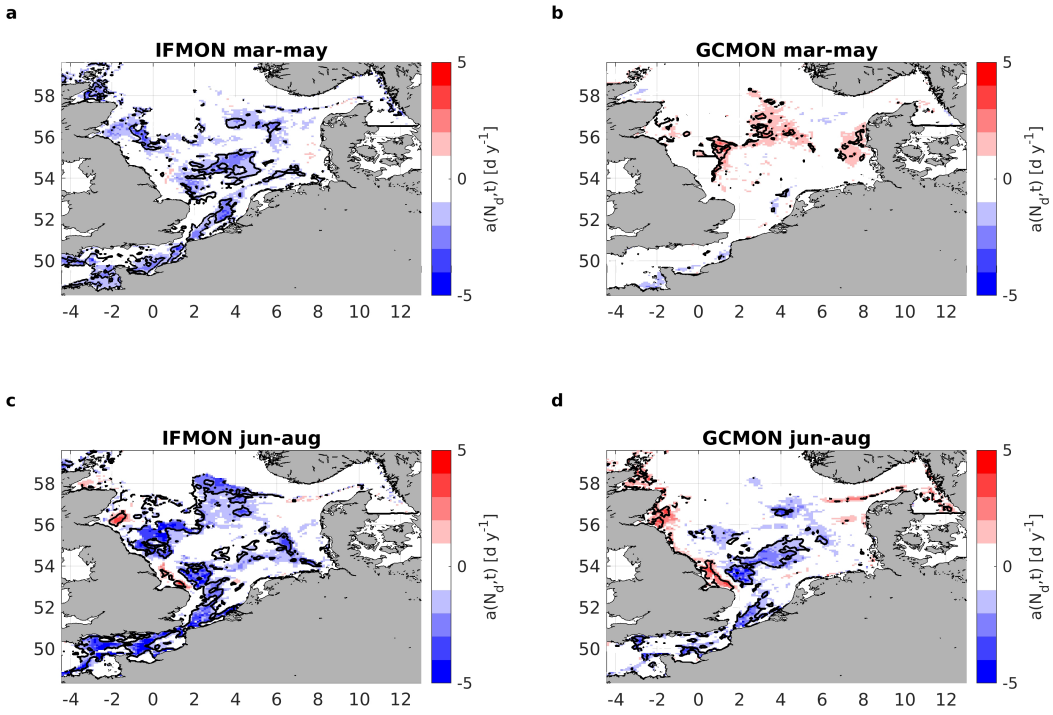

Figure 12. Slopes of N_d for IFMON (left column) and GCMON (right column) for the seasons of spring (top row) and summer (bottom row). Blanked out areas are where the slope has been found insignificant via the t-test ($p > 0.05$). The black contour line denotes $R^2 > 0.2$.

Sea, up until about a latitude of $53°N$, west of the island of Texel in the Netherlands. The IFREMER data set was calibrated for the English Channel and is therefore likely to be accurate there. The GlobColour data on the other hand, although showing slight but weakly significant increases in SPM in the English Channel as well, showed predominantly decreases most everywhere else. Particularly of note is an area to the east of England, where the IFREMER data also shows a slight decrease. As is shown in Appendix B and figure 2, GlobColour tends to estimate SPM lower than IFREMER. In summary, question (I) is answered positively, yet we advise against claiming that this constitutes evidence of actual changes. Further investigation, incorporating in-situ measurements is strongly recommended.

Secondly, we asked whether trends in SPM directly caused trends in water clarity (II). It was shown that in many, yet not in all cases, statistically significant changes in z_{10} occured often where trends in SPM were found. Generally speaking, where there were increases in SPM, there was a shallowing (i.e., a positive change) in z_{10}, and a deepening for decreases. IFMON showed almost exclusively shallowing, except for mainly the aforementioned region east of England, where GCMON shows shallowing as well, yet stronger. Furthermore, GCMON showed a statistically highly significant deepening north of $55°N$ and west of $2°E$, which is to be looked at with caution due to its location in the far North and the already large magnitudes of z_{10} in this area. Still, the 20-year slope there is $-0.5m/y$, i.e., $\approx 10m$ over the entire timespan. In several regions, e.g., south of the Dogger Bank (around $54°N$), there was a shallowing in both IFMON and GCMON, although only the IFREMER data showed increases in SPM, and rather on the Dogger Bank than to the south of it. This, again, hints at a drift between the two SPM data sets. In conclusion, there are changes in z_{10} that can be linked directly to changes in SPM, as well as others where the causal link is very likely.

Thirdly, we asked whether there was a significant change in phytoplankton biomass. For GCMON, this was not the case. For IFMON, there were statistically significant declines, particularly for the southern North Sea and the English Channel, where SPM had declined and z_{10} had shoaled. The amount of the decline in P_{10} was in orders of 10% (not shown). It is noticeable that increasing SPM and shoaling z_{10} appear to be linked with decreases in P_{10}, yet, as the GCMON results show, the opposite is not the case. Furthermore, it is not true everywhere. A likely hypothesis is that the impact of light limitation is strongest where nutrient limitation is lowest. Further investigations into the causes of these declines are thus advisable. Nevertheless, the answer to question (III) is that for regions of high nutrient availability, a darkening of the light climate could cause declines in phytoplankton biomass.

Whether there was a noticeable change in bottom illumination was the subject of question (IV). It was indeed the case that several regions showed significant changes in bottom illumination in both IFMON and GCMON. We analyzed only the seasons of spring and summer, for the previously mentioned reasons of low data availability and potentially high errors in winter and autumn. In the season of spring, the two experiments showed little to no agreement. By tendency, GCMON showed increases and IFMON decreases. However, in summer, the agreement was much better, particularly in the western and southern North Sea, although decreases were still stronger for the most part in IFMON. GCMON on the other hand showed increases along the eastern shore of Great Britain, which were present but weaker in IFMON. On the other hand, IFMON showed strong decreases in the English Channel, which were also there in GCMON, albeit at lower intensity. Note that overall, the largest possible increase or decrease over the studied 18 years would be $5dy^{-1}$, assuming a length of $90d$ per season. In this case, the bottom illumination would have gone from no illumination at all to full illumination, or vice versa, respectively. This was indeed the case in both runs, particularly for the area between $0°E$ and $3°E$, and $53°N$ and $55°N$.

The fifth research question concerns itself with consistency in regard to other research. Capuzzo et al. (2015) carried out statistical analysis on SPM and chlorophyll in-situ data over the period of 1988 to 2011. They found increases in SPM for several regions, while chlorophyll on the other hand was found to not change significantly for the most part (their figure 4 - note that only the columns representing spring/autumn and summer are comparable). They divided the North Sea into regions of hydrodynamical likeness, i.e., there was a region defined as seasonally stratified, one was named freshwater influence (the Rhine plume), another the East Anglia plume, a permanently mixed region along the south western shores and intermediate waters, which was every other region of the North Sea between $51°N$ and $57°N$. The increases in the in-situ SPM were particularly strong in the East Anglia plume, where our results show only few significant trends. Only the IFREMER data showed increases there, albeit of low statistical significance. In fact, the GlobColour data shows decreases only, which would be in contradiction to the results of Capuzzo et al. (2015).

Dupont & Aksnes (2013) corrected for topographic effects of bottom depth and distance to shore via a two-variable linear regression to derive centennial trends (1903-1998) in Secchi-depth. They found a decrease in residual Secchi-depth (i.e., observed minus modelled Secchi-depth) by $3.1\pm0.2m$, and a decrease of $4.6\pm0.02my^{-1}$ for the uncorrected data. This corresponds to an annual decrease of $0.33\pm0.02my^{-1}$, or $0.058\pm0.02my^{-1}$, respectively. Following Lee et al. (2015), Secchi-depth is proportional to $|z_{10}|$ by a factor of $\approx$ 0.43. The average change in z_{10} (not filtering the trends for significance, for better comparability) was $0.278\pm0.186my^{-1}$ for IFMON and $-0.018\pm0.086my^{-1}$ for GCMON, which corresponds to a change in Secchi-depth of $0.12\pm0.08my^{-1}$ and $-0.008\pm0.037m^{-1}$. Therefore, assuming the numbers of Dupont & Aksnes (2013) are accurate, IFMON exhibits a trend that is about four times as large as their data, while GCMON exhibits no significant change at all when averaged over the entire basin. It is therefore negligent to assume that either run is an accurate simulation of reality. Instead, this serves to emphasize the importance of cross-referencing the SPM data to other sources. How-

ever, directionally speaking, the changes in IFMON appear to match those in Dupont & Aksnes (2013) better. Both Dupont & Aksnes (2013) and Capuzzo et al. (2015) found an overall decrease in clarity in the North Sea. On the other hand, Alvarez-Fernandez & Riegman (2014) found increasing trends in photosynthetically available radiation (PAR) in the Dutch North Sea over the period of 1990-2010, hinting at changes in optically active constituents, on the causes of which, they do not make a claim. Their findings would, however, contradict the shallowing trends of z_{10} in IFMON, while not contradicting behaviour in GCMON. The findings of Dupont & Aksnes (2013) and Capuzzo et al. (2015) appear to indicate the validity of the results for IFMON. We therefore must leave question (V) with an ambiguous answer. While some results may agree with some findings in literature, there is no generality and no certain answer to the overarching question whether the North Sea is getting more turbid. We therefore do not claim to contribute to the answer of this particular question in either direction.

4.2 Validity of the Method

By using offline non-living SPM data, we simplify what otherwise would potentially be very costly, because we do not need to run a sediment and wind wave model coupled alongside ROMS-CoSiNE. We instead make use of satellite-derived data that has been shown to be reliable for both case 1 waters (Gohin et al., 2005) and case 2 waters (Gohin, 2011). This ensures well represented long-term sediment dynamics, and consistency between long-term sediment dynamics and trends in the model. The employment of two data sets serves to demonstrate the validity of the method, showing that trends in z_{10} in the model are indeed caused by trends in the SPM data. Furthermore, it expands the benefits and use of remotely sensed data in modelling. Sediment models are not always reliable and a 20-year simulation poses an exceptional challenge.

The algorithm that is used to generate the satellite data utilises in-situ data, which in itself may be of varying quality. Röttgers et al. (2014) provide an overview over issues which frequently arise with in-situ SPM data and measurement uncertainties, such as salt aggregation at filter margins or filter material loss. The impact that systematic errors in-situ SPM data have on the satellite product is hard to determine. See Appendix B for a comparison of the two satellite products employed against in-situ data, collected by Rijkswaterstaat in the Netherlands. Both data sets tend to underestimate SPM relative to the in-situ measurements, and more so for the GlobColour data, however, as is elaborated on in the same section, there are explanations for these discrepancies.

Even when the in-situ data is guaranteed to be consistently of high quality, the properties of the suspended matter, such as particle size, composition or density may vary over time, which will affect the validity of the satellite algorithm's calibration (Twardowski et al., 2001; Gallegos et al., 2011; Bowers et al., 2017). Remote sensing reflectance is primarily a function of SPM floc cross-sectional area, rather than mass. The floc cross-sectional area, however, is itself dependent on the concentration of organic matter. Balasubramanian et al. (2020) have derived an algorithm which distinguishes between three different water types (blue, green and brown), which may help to adapt to changing SPM properties over time, yet it still requires in-situ data for calibration and refinement. Such effects of systematic changes are common in coastal waters, particularly, and are likely to have occurred over the 20^{th} century (comapare e.g. Capuzzo et al., 2015). Furthermore, as Gallegos et al. (2011) point out, even if the remote sensing reflectance remains constant at one location for a particular amount of time, the ratio of scattering to absorption may still change. In fact, they concluded that over the period of 1987-2009, Secchi depth had declined, due to decreasing backscattering ratios, while measured remote sensing reflectance remained effectively constant. The changes in Secchi depth and backscattering were associated with organic particles, particularly with small organic detritus. Contributions of mineral particles were ruled out. This also indicates that the optical penetration depth (which is related to Secchi depth) may change, even though remote sensing reflectance may remain constant.

Our model does not consider CDOM specific attenuation. Although there is a version of CoSiNE that does compute CDOM as a state variable (Xiu & Chai, 2014), the version used in this study does not. However, since we focus on the effects of sediment changes, we neglect CDOM at this point for the same reason that we use climatological river forcing, for introducing further complexity. Inclusion of CDOM is an obvious next step to take. While there are many possible ways of achieving this, e.g., through modelling (e.g. Kerimoglu et al., 2020, most recently) or via an inverse relation with salinity (e.g. Wollschläger et al., 2020), it is worth noting that the same method by which we introduce SPM in this study is in theory applicable for satellite-derived CDOM data as well. Such is available e.g. from GlobColour (`http://www.globcolour.info/`). Wakelin et al. (2012) used a comparable method of introducing non-algal light attenuation, by combining both SPM and CDOM specific attenuation into a standalone model variable, a_{det}. It is then relaxed against observational data from SeaWiFS, and transported along like all other properties. An obvious upside to this approach is that it allows for higher temporal resolution (they use 7-day intervals).

Making use of two data sets, which are generated via the same principal algorithm (Gohin et al., 2005; Gohin, 2011), we found that they differ in a number of places. As was shown in figure 5, there may be differences in magnitude and seasonal behaviour. The linear regression of annual means showed significant increases in SPM for the IFREMER data set particularly in regions deeper than $40m$ and scarcely any trends in the southern North Sea, while the GlobColour data set showed no significant trends only in a number of regions of the shallower, southern North Sea (figure B4). Note here that the IFREMER data set shows highly linear trends in time, particularly in the northern regions with$R^2 > 0.7$ in some cases. Thus, one might be tempted to assume a strong increase in SPM. This is however entirely absent in the GlobColour data set and is likely caused by errors due to low data coverage and, subsequently, spurious interpolation. In the few occurrences of overlapping areas, i.e. areas that show trends in both data sets, they may be in opposite directions, e.g., around $55°N$ and $0.5°E$.

Using annual means is not appropriate for long-term simulations such as the here presented, as the SPM rich winter months bias SPM upwards in the growing season, where it is usually much lower. This leads to z_{10} being much shallower, i.e., the water being much more turbid in IFANN than in IFMON. Due to the affordability of this method, it is generally unadvisable to use any lower frequency than monthly means. Ideally, the SPM input should come in at least at a synoptic frequency, i.e. 3-7 days. However, the sparsity of data due to cloud coverage would then require sophisticated interpolation. The method used by Wakelin et al. (2012) can bridge data gaps and is potentially preferable to our method when aiming for high frequency response in SPM. However, for long-term analyses, this takes away the benefit of efficiency that employing offline forcing has. As a potential consequence of using too low of a temporal resolution, errors in spring bloom timing may occur. Recently, Opdal et al. (2019) have demonstrated the role that light limitation plays in the timing and triggering the spring bloom. If for any hypothetical year the temperature and nutrient conditions were favorable for an early spring bloom, yet because of a storm event several weeks earlier, the monthly averaged SPM in our model would, erroneously, be very high, it might delay the spring bloom due to light limitation. Thus, when focussing on spring bloom timing, high frequency SPM input, e.g., from a model is preferable. A combined approach, e.g. the one described by Wakelin et al. (2012), or any other viable combination of model, satellite and in-situ data will undoubtedly be preferable in some cases. This work may serve as a stepstone towards such approaches.

We performed the linear regression on the spring and summer seasons, thereby excluding those months where data scarcity would bias the analysis. Furthermore, the spring bloom in any of our runs occurs earliest in March. There seldomly is growth after September. The bulk of all phytoplankton growth is therefore captured inside this time window. Due to higher data coverage of SPM, we consider the given data to be reliable within the same window and thus it is possible to investigate links between SPM, water clarity, and phytoplankton growth during this time.

In section 2.3, we made several simplifying assumptions. One was that SPM was vertically homogeneous. As was also stated there, this likely leads to an underestimation of SPM, which, due to its sinking, tends to accumulate near the bottom. We furthermore made the assumption that at times when SPM was the highest, the water column was likely well mixed. This does not need to be the case at all times. However, the resulting error in the photosynthetic rate are assumed to be small, as these higher concentrations of SPM will likely be below the photic depth. Furthermore, there is no sound method to extrapolate SPM downwards without adding additional uncertainty.

The SPM data has been used to validate sediment models in the past, for which purpose it has proven its worth. In Sykes & Barciela (2012), a 3D operational model (the Medium Resolution Continental Shelf, MRCS), consisting of a hydrodynamic and sediment component (Proudman Oceanographic Laboratory Coastal Ocean Modelling System, POLCOMS), and ERSEM as the biological module was validated using the same satellite product, as well as CEFAS (Centre for Environment, Fisheries and Aquaculture Science) SmartBuoy data. The satellite data was found to be in good agreement with the SmartBuoy turbidity data (their figures 2 and 3), and served to improve the model. The MRCS is the precursor to AMM7-ERSEM. The data was also used for validation of a 3D ROMS application in the English Channel (Guillou et al., 2015). Our approach is a relatively novel one. Thus, these aforementioned studies are not directly comparable to ours. However, they serve to show how the data can be used to improve models. Furthermore, while this does not imply that satellite data are equivalent to in-situ data, qualitatively speaking, they are comparable to the output of sediment models.

The analysis error of the satellite data undergoes a clear seasonal cycle, particularly in the south of the domain, which is shown in figure B2, where monthly climatologies of data errors are shown. figure B3 shows the same, except divided by the monthly climatology of SPM, yielding a relative error, which reveals that due to the generally low levels of SPM in the northern North Sea, the analysis error is consistently in the same orders as the actual monthly climatology. Those are the very regions in which the most significant trends in SPM and z_{10} were found, when analysing trends in annual averages (see figure B4 and B5). However, the absolute errors are consistently highest in winter months, i.e. outside the growing season. Using offline SPM enables us to perform a long-term analysis in the first place, as we can be sure that trends in the SPM data are not due to intrinsic modelling errors or biases. Note that there are modelling approaches that are more affordable than common sediment models (van der Molen et al., 2017). However, as being able to achieve consistent SPM data over 20 years is paramount, the use of satellite data is simpler in set-up and application. Biological models that use neither offline nor online SPM data for sediment specific attenuation are in any case unrealistic. It has been shown that horizontal variability of water clarity is easy to achieve in modelling and can also be very affordable (Thewes et al., 2020).

In section 1, we defined N_d as the number of days in which the irradiance at the bottom was larger than 1% of the surface irradiance. Owing to our assumption that SPM was vertically homogeneous, we neglect effects of increased attenuation that is bound to occur near the bottom. As e.g. (Sanford & Lien, 1999) show, for tidally impacted areas, turbulent kinetic energy dissipation rates are highest in regions lower than $10m$ above the bottom, causing fast sinking sediments to seldomly be re-suspended much higher. A quantity that might be called "near-bottom illumination", which is the number of days when $|z_1| > |H - 10m|$, where H is the bottom depth, would be more realistic and comparable with in-situ measurements of bottom illumination. This would not drastically change the results of the long-term analysis, qualitatively speaking. Yet, as the condition for near-bottom illumination is obviously more likely to be true, it might make linear regression less applicable, because the natural upper limits of $N_d = 366d$, or $\approx 90d$ for separate seasons, may be reached more quickly, at which point N_d remains constant. For purposes of ecological modelling, however, particularly when there is a benthic module, N_d, as it is defined in this study, is the more relevant number. In essence, it can be

understood as a theoretical upper limit to the number of days where bottom illumination can occur.

5 Conclusions

In this study, we made use of two data sets of satellite-derived non-algal SPM, to analyze the effect of long-term changes in SPM on water clarity and phytoplankton biomass. While intuitively, one might have presumed that the more SPM there is, the more turbid the water and the lower the phytoplankton growth is, we have shown that this need not always be the case. While we do not go into definitive detail as to why this is, we deem interplay between light and nutrient limitation a likely factor.

We could not identify clear trends for both data sets, which emphasizes the need for further investigation into this topic. Particularly, since the two data sets used the same principal algorithm, it needs to be noted that satellite-derived SPM is not to be understood as equivalent to in-situ or modelled SPM. Particularly in coastal regions, there have been advances made in the past decade, which will likely improve the quality of satellite products (e.g. Balasubramanian et al., 2020; Vanhellemont & Ruddick, 2021). Follow up studies to ours may therefore lay their focus on the changes such improvements bring about, and perhaps form a clearer picture of whether or not the North Sea actually is getting more turbid. Of course, similar studies might be prudent for other regions of the world as well. Nevertheless, our work provides a starting point with establishing that long-term changes in sediment do bring about long-term changes in the light climate and to the ecosystem in general.

Bottom illumination changed noticeably in summer in both IFMON and GCMON. While along the British East Coast, the number of illuminated days increased, there were strong decreases in the English Channel and south of the Dogger Bank. Our results suggest that it is possible for a region to change from the bottom being fully illuminated for an entire season to not illuminated at all within the time span of two decades. This could have severe consequences for the benthic ecosystem. While our results cannot be seen as conclusive, they do motivate a thorough investigation, incorporating of field data.

Appendix A Model parameters

Table A1. CoSiNE Parameters

Parameter	Symbol	Value	Unit
Light attenuation of pure water	k_W	0.36	m^{-1}
Light attenuation due to phytoplankton	k_P	0.03	$m^{-1}(mmolm^{-3})^{-1}$
Light attenuation due to SPM	k_{SPM}	0.066	$m^{-1}(gm^{-3})^{-1}$
Initial slope of P-I curve for P1	α_{P1}	0.05	$d^{-1}(Wm^{-2})^{-1}$
Initial slope of P-I curve for P2	α_{P2}	0.1	$d^{-1}(Wm^{-2})^{-1}$
Photo-inhibition slope for P1	$beta_{P1}$	80	Wm^{-2}
Photo-inhibition slope for P2	$beta_{P2}$	100	Wm^{-2}
Nitrification rate	γ_7	0.25	d^{-1}
Max. specific growth of P1	$\mu_{1,max}$	2.0	d^{-1}
Max. specific growth of P2	$\mu_{2,max}$	3.0	d^{-1}
Ammonium inhibition parameter	ψ	4.0	$(mmolNH4m^{-3})^{-1}$
Half-saturation for NO3 uptake by P1	$Kno3p1$	1.0	$mmolNO3m^{-3}$
Half-saturation for NO3 uptake by P2	$Kno3p2$	3.0	$mmolNO3m^{-3}$
Half-saturation for NH4 uptake by P1	$Knh4p1$	0.1	$mmolNH4m^{-3}$
Half-saturation for NH4 uptake by P2	$Knh4p2$	0.3	$mmolNH4m^{-3}$
Half-saturation for PO4 uptake by P1	$Kpo4p1$	0.1	$mmolPO4m^{-3}$
Half-saturation for PO4 uptake by P2	$Kpo4p2$	0.2	$mmolPO4m^{-3}$
Half-saturation for SiOH4 uptake by P2	$Ksioh4p2$	4.5	$mmolSiOH4m^{-3}$
Half-saturation for oxidation	KO	30	$mmolOm^{-3}$
P1 specific mortality rate	γ_3	0.2	d^{-1}
P2 specific mortality rate	γ_4	0.1	d^{-1}
Max. grazing rate of Z1	$G_{1,max}$	1.6	d^{-1}
Max. grazing rate of Z2	$G_{2,max}$	0.75	d^{-1}
Half-saturation for Z1 grazing	$K_{1,max}$	0.3	$mmolNm^{-3}$
Half-saturation for Z2 grazing	$K_{2,max}$	0.2	$mmolNm^{-3}$
Z2 specific mortality rate	γ_0	0.1	d^{-1}
Z1 excretion rate	reg_1	0.2	d^{-1}
Z2 excretion rate	reg_2	0.1	d^{-1}
Z1 grazing efficiency	γ_1	0.75	1
Z2 grazing efficiency	γ_2	0.75	1
Z2 grazing preference for P1	ρ_5	0.7	1
Z2 grazing preference for Z1	ρ_6	0.2	1
Z2 grazing preference for detritus	ρ_7	0.1	1
Decay rate of silicic detritus	γ_5	0.2	d^{-1}
Dissolution rate for nitrogeneous detritus	γ_6	2.0	d^{-1}
Sinking velocity for nitrogeneous detritus	$w_{s,dN}$	15	md^{-1}
Sinking velocity for silicic detritus	$w_{s,dS}$	25	md^{-1}
Sinking velocity for P2	$w_{s,P2}$	1.0	md^{-1}

Appendix B SPM uncertainties

Along with the SPM data, the IFREMER data set provides an analysis error, and we averaged it to a monthly frequency, the same way we did with the actual SPM data. figure B1 shows a monthly climatology of SPM for 1998-2017. Figure B2 shows climatological monthly means for the analysis error, and figure B3 shows the same, divided by climatological monthly means of SPM. Note the high values in the northern North Sea for all three quantities, which are due to data sparsity, caused by cloud cover.

For demonstrational purposes in relation to figure 7, figure B4 shows the same, i.e., regression slopes of SPM data, but averaged annually instead of over spring and summer months. This helps to visualize the necessity for seasonal filtering, because the winter months contribute heavily to the long-term trends, even though they have little relevant effects on phytoplankton growth, and they are known to be error prone. Likewise, figure B5 shows the same as figure 8, except averaged annually.

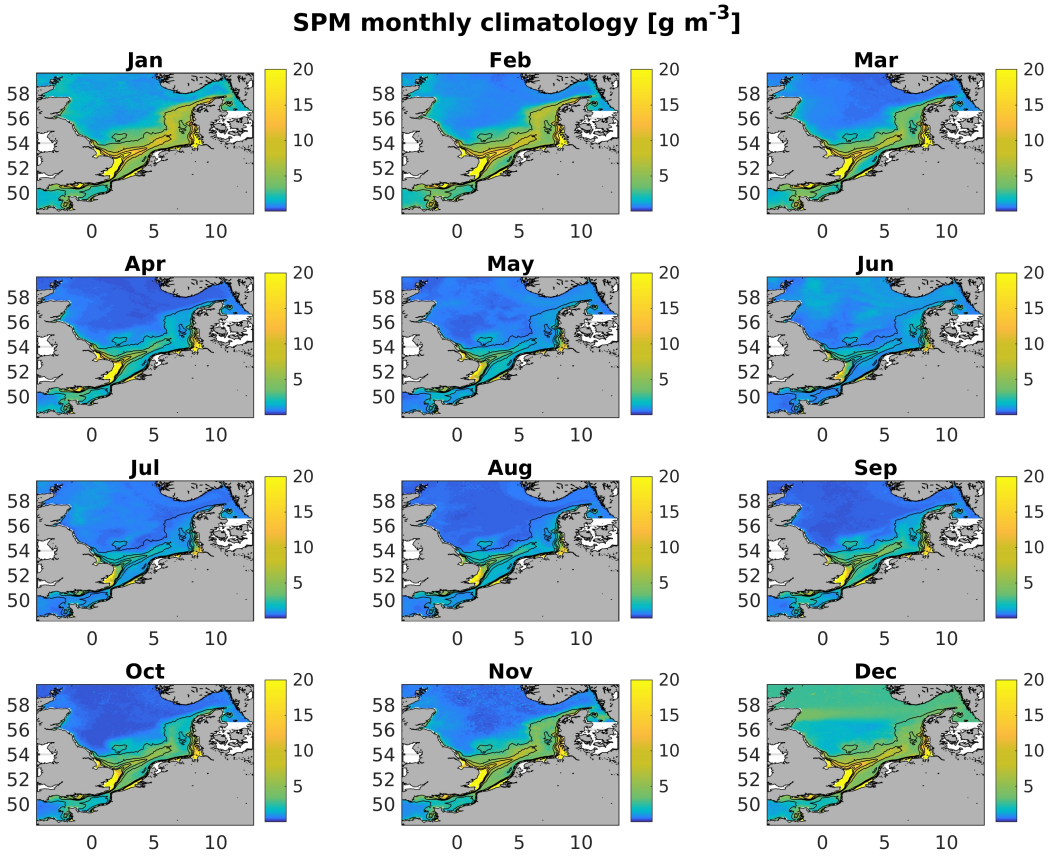

Figure B1. Monthly climatology of SPM for 1998-2017.

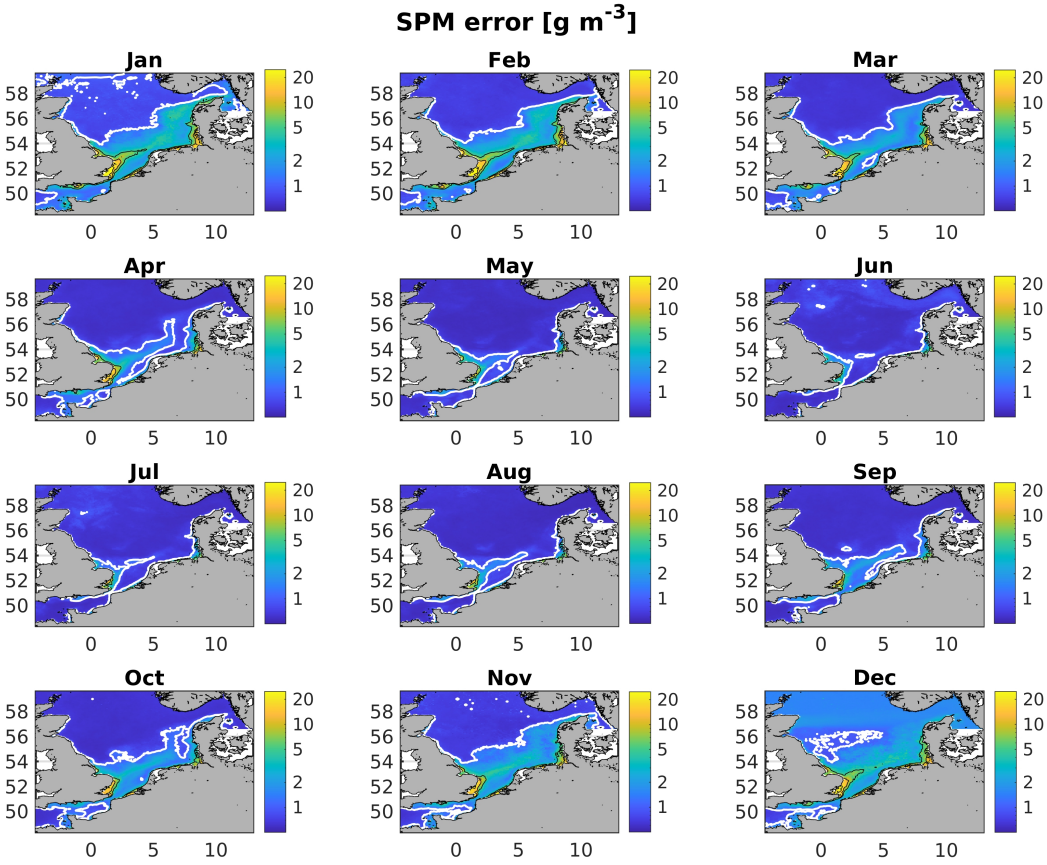

Figure B2. Monthly climatology of SPM analysis error for 1998-2017. The white contour line denotes an error of $1gm^{-3}$. Black contour lines denote values of 5, 10, 20 and $30gm^{-3}$.

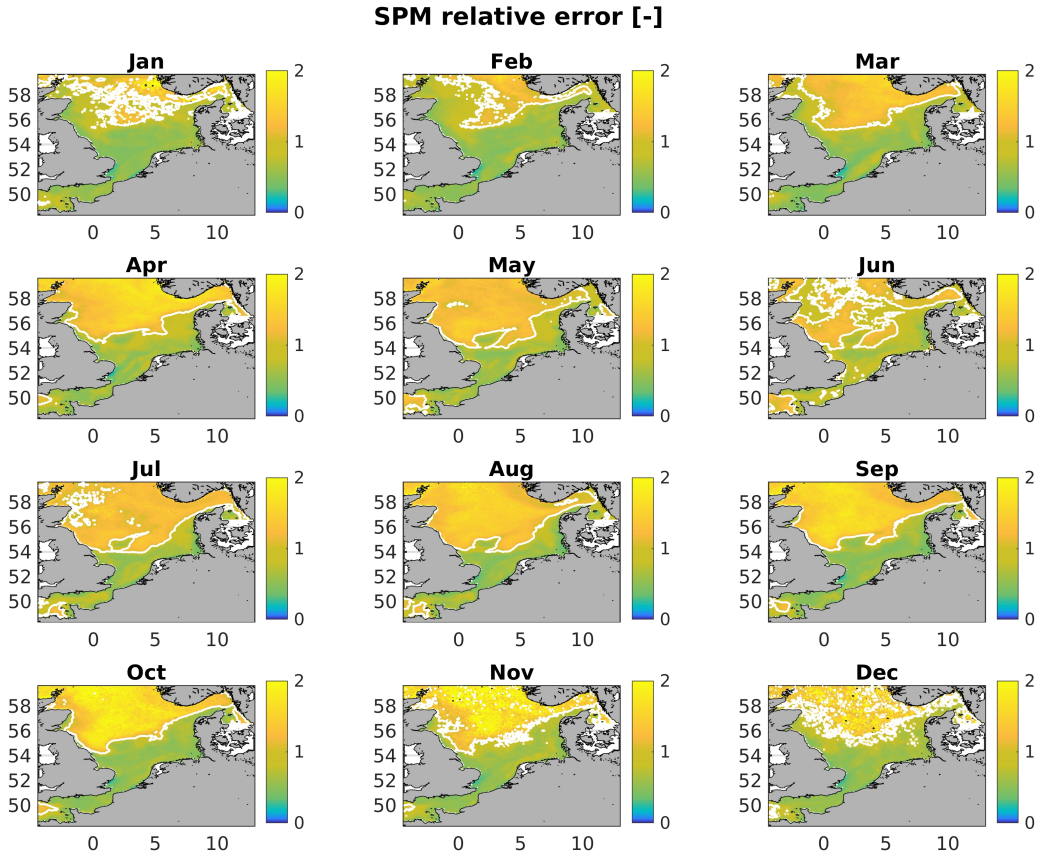

Figure B3. Monthly climatology of relative SPM analysis error for 1998-2017. The white contour line denotes a relative error of 1.

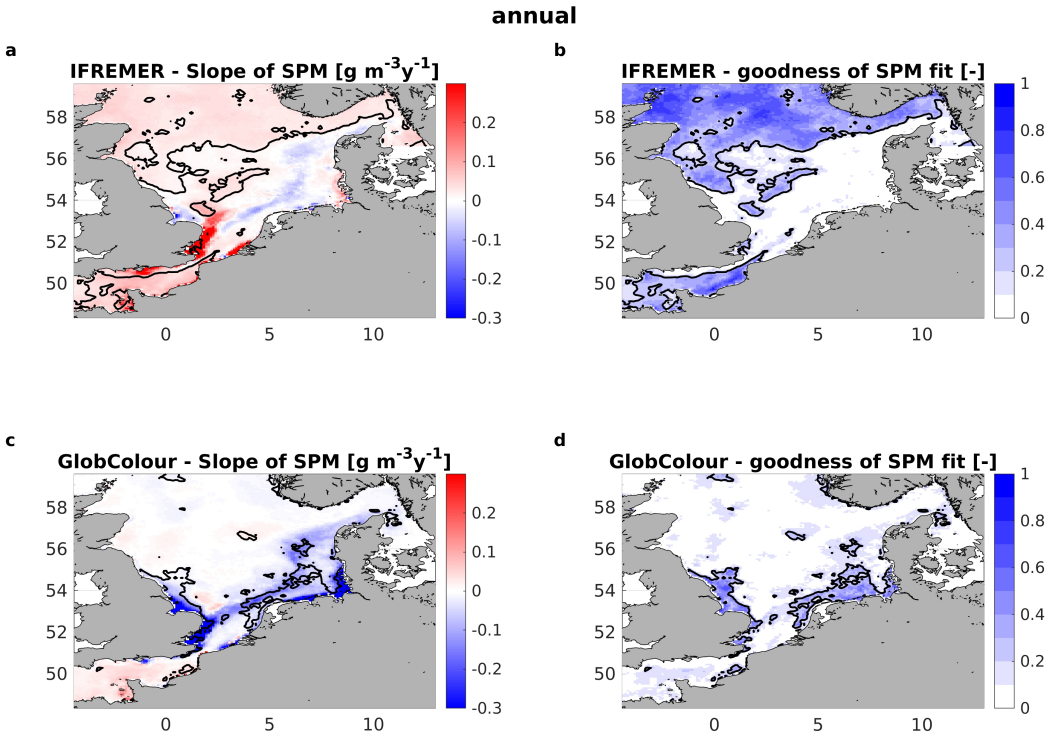

Figure B4. Linear regression slopes (a&c) and R^2 (b&d) for IFREMER (top row) and GlobColour (bottom) SPM data, annually averaged. The solid black contour lines mark where $p < 0.05$.

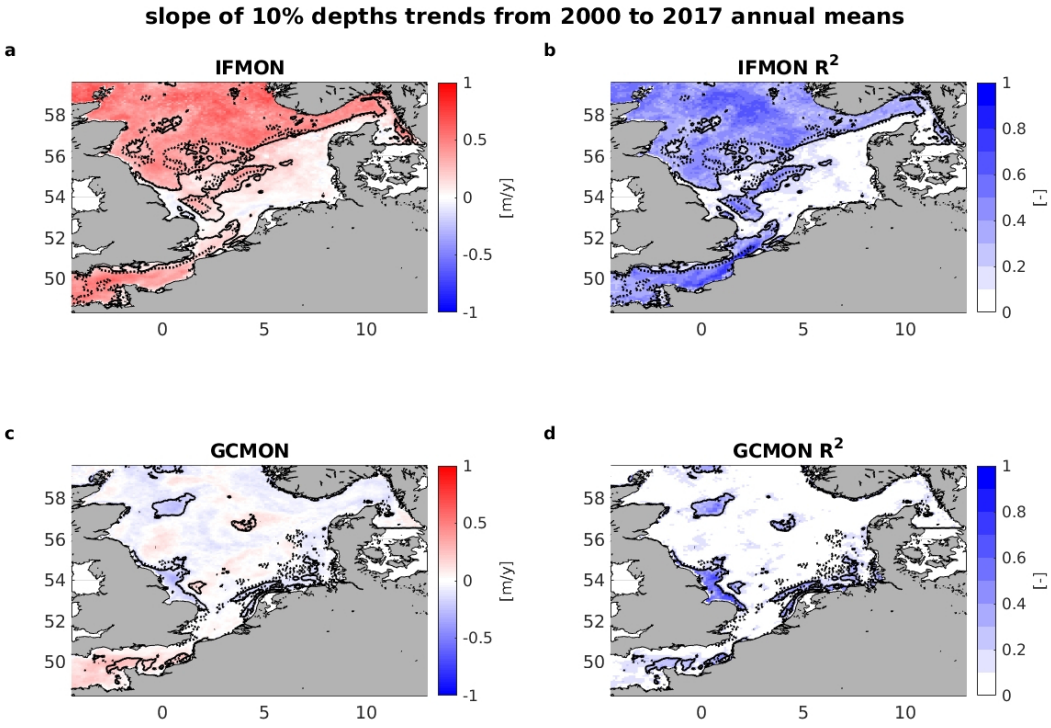

Figure B5. Linear regression slopes (a&c) and R^2 (b&d) for IFMON (top row) and GCMON (bottom) z_{10}, annually averaged. The solid black contour lines mark where $p < 0.05$.The dotted black contour lines denote where the respective SPM data showed significant trends (compare fig. B4).

Acknowledgments

This work was carried out within the project Coastal Ocean Darkening (grant no. ZN3175), funded by the Ministry of Science and Culture of the German federal state of Lower Saxony. DFKI acknowledges financial support by the MWK through Niedersachsen Vorab (ZN3480).

The satellite-derived SPM data used was provided by IFREMER (2017) and is available at `https://sextant.ifremer.fr/record/adf985c6-95e7-48ce-9b2b-083f1e5860eb/`. GlobColour data (`http://globcolour.info`) used in this study has been developed, validated, and distributed by ACRI-ST, France. This study has been conducted using E.U. Copernicus Marine Service Information, which is available at `https://marine.copernicus.eu/`. The code used to compute FES2014, was developed in collaboration between Legos, Noveltis, CLS Space Oceanography Division and CNES, and is available under GNU General Public License. Atmospheric forcing data was provided by the NOAA ESRL Physical Sciences Division, Boulder, Colorado, USA, and taken from their website at `https://psl.noaa.gov/data/`. The data used for validation was provided by the International Council for the Exploration of the Sea (ICES), Copenhagen (2014). The ICES Data set on Ocean Hydrography is available at `https://www.ices.dk/data/Pages/default.aspx`. The in-situ data used for comparison against satellite data was provided by Rijkswaterstaat, Netherlands (`https://opendap.deltares.nl/thredds/catalog/opendap/rijkswaterstaat/waterbase/30_Zwevende_stof_in_mg_l_in_oppervlaktewater/nc/catalog.html`). Data generated in this study are available at `https://uol.de/icbm/kuestenforschung/thewes-cod`. The satellite data, interpolated to match the in-situ data points may also be found there.

We thank Hajo Krasemann, Fei Chai, Feng Zhou, Francis Gohin, Jochen Wollschläger, Jaime Pitarch, Matthias Schröder, Sebastian Grayek and Johannes Pein for helpful insights, comments and support.

References

Alvarez-Fernandez, S., & Riegman, R. (2014). Chlorophyll in north sea coastal and offshore waters does not reflect long term trends of phytoplankton biomass. *Journal of Sea Research*, *91*, 35–44. Retrieved from `https://www.sciencedirect.com/science/article/pii/S138511011400077X` doi: 10.1016/j.seares.2014.04.005

Balasubramanian, S., Pahlevan, N., Smith, B., Binding, C., Schalles, J., Loisel, H., ... Boss, E. (2020). Robust algorithm for estimating total suspended solids (tss) in inland and nearshore coastal waters. *Remote Sensing of Environment*, *246*. doi: 10.1016/j.rse.2020.111768

Baretta, J., Ebenhöh, W., & Ruardij, P. (1995, July). The European regional seas ecosystem model, a complex marine ecosystem model. *Netherlands Journal of Sea Research*, *33*(3-4), 233–246.

Blackford, J., Allen, J., & Gilbert, F. (2004, December). Ecosystem dynamics at six contrasting sites: a generic modelling study. *Journal of Marine Systems*, *52*(1-4), 191–215. doi: 10.1016/j.jmarsys.2004.02.004

Bowers, D. G., McKee, D., Jago, C. F., & Nimmo-Smith, W. A. M. (2017). The area-to-mass ratio and fractal dimension of marine flocs. *Estuarine, Coastal and Shelf Science*, *189*, 224–234. Retrieved from `https://www.sciencedirect.com/science/article/pii/S0272771416304565` doi: https://doi.org/10.1016/j.ecss.2017.03.026

Cahill, B., Schofield, O., Chant, R., Wilkin, J., Hunter, E., Glenn, S., & Bisset, P. (2008, May). Dynamics of turbid buoyant plumes and the feedbacks on nearshore biogeochemistry and physics. *Geophys. Res. Lett*, *35*(10).

Capuzzo, E., Lynam, C., Barry, J., Stephens, D., Forster, R., Greenwood, N., ... Engelhard, G. (2018). A decline in primary production in the North Sea over

25 years, associated with reductions in zooplankton abundance and fish stock recruitment. *Global Change Biology*, *24*(1). doi: 10.1111/gcb.13916

Capuzzo, E., Stephens, D., Silva, T., Barry, J., & Forster, R. (2015, January). Decrease in water clarity of the southern and central North Sea during the 20th century. *Global Change Biology*, *21*(6), 2206–2214. doi: 10.1111/gcb.12854

Chai, F., Dugdale, R., Peng, T.-H., Wilkerson, F., & Barber, R. (2002). One-dimensional ecosystem model of the equatorial Pacific upwelling system. Part I: model development and silicon and nitrogen cycle. *Deep Sea Res. II: Top. Stud. Oceanogr.*, *49*(13-14), 2713–2745.

Dupont, N., & Aksnes, D. (2013, October). Centennial changes in water clarity of the Baltic Sea and the North Sea. *Estuarine, Coastal and Shelf Science*, *131*(10), 282–289. doi: 10.1016/j.ecss.2013.08.010

Gallegos, C., Werdell, P. J., & McClain, C. (2011). Long-term changes in light scattering in chesapeake bay inferred from secchi depth, light attenuation, and remote sensing measurements. *Journal of Geophysical Research: Oceans*, *116*(C7). Retrieved from `https://agupubs.onlinelibrary.wiley.com/doi/abs/10.1029/2011JC007160` doi: https://doi.org/10.1029/2011JC007160

Gohin, F. (2011, October). Annual cycles of chlorophyll-a, non-algal suspended particulate matter, and turbidity observed from space and in-situ in coastal waters. *Ocean Science*, *7*, 705–732. doi: 10.5194/os-7-705-2011

Gohin, F., Loyer, S., Lunven, M., Labry, C., Froidefond, J., Delmas, D., ... Herbland, A. (2005). Satellite-derived parameters for biological modelling in coastal waters: Illustration over the eastern continental shelf of the Bay of Biscay. *Remote Sensing of Environment*, *95*(1), 29–46. doi: 10.1016/j.rse.2004.11.007

Gohin, F., van der Zande, D., Tilstone, G., Eleveld, M., Lefebvre, A., Andrieux-Loyer, F., ... Saulquin, B. (2019). Twenty years of satellite and in situ observations of surface chlorophyll-a from the northern Bay of Biscay to the eastern English Channel. Is the water quality improving? *Remote Sensing of Environment*, *21*, 111343. doi: 10.1016/j.rse.2019.111343

Guillou, N., Rivier, A., Gohin, F., & Chapalain, G. (2015, 5). Modelling near-surface suspended sediment concentration in the english channel. *Journal of Marine Science and Engineering*, *2*, 193–215. doi: 10.3390/imse3020193

Haidvogel, D., Arango, H., Hedstrom, K., Beckmann, A., Malanotte-Rizzoli, P., & Shchepetkin, A. (2000, August). Model evaluation experiments in the North Atlantic Basin: simulations in nonlinear terrain-following coordinates. *Dyn. Atmos. Ocean*, *32*(3-4), 239–281.

IFREMER. (2017). *Matières en suspension minérales interpolées (données satellite).* doi: 10.12770/adf985c6-95e7-48ce-9b2b-083f1e5860eb

Kerimoglu, O., Voynova, Y. G., Chegini, F., Brix, H., Callies, U., Hofmeister, R., ... van Beusekom, J. E. E. (2020). Interactive impacts of meteorological and hydrological conditions on the physical and biogeochemical structure of a coastal system. *Biogeosciences*, *17*(20), 5097–5127. Retrieved from `https://bg.copernicus.org/articles/17/5097/2020/` doi: 10.5194/bg-17-5097-2020

Lee, Z., Shang, S., Hu, C., Du, K., Weidemann, A., Hou, W., ... Lin, G. (2015, November). Secchi disk depth: A new theory and mechanistic model for underwater visibility. *Remote Sensing of Environment*, *169*, 139–149. doi: 10.1016/j.rse.2015.08.002

Liu, Q., Chai, F., Dugdale, R., Chao, Y., Xue, H., Rao, S., ... Zhang, Y. (2018, June). San Francisco Bay nutrients and plankton dynamics as simulated by a coupled hydrodynamic-ecosystem model. *Continental Shelf Research*, *161*, 29–48. doi: 10.1016/j.csr.2018.03.008

Marchesiello, P., McWilliams, J., & Shchepetkin, A. (2001). Open boundary conditions for long-term integration of regional ocean models. *Ocean Modelling*, *3*, 1–20. doi: 10.1016/S1463-5003(00)00013-5

Mason, E., Molemaker, J., Shcheptkin, A., Colas, F., McWilliams, J., & Sangrà, P. (2010). Procedures for offline grid nesting in regional ocean models. *Ocean Modelling*, *35*, 1–15. doi: 10.1016/j.ocemod.2010.05.007

Mobley, C., Chai, F., Xiu, P., & Sundman, L. (2015, January). Impact of improved light calculations on predicted phytoplankton growth and heating in an idealized upwellingdownwelling channel geometry. *Journal of Geophysical Research*, *120*(2), 875–892. doi: 10.1002/2014JC010588

O'Dea, E., Arnold, A., Edwards, K., Furner, R., Hyder, P., Martin, M., ... Liu, H. (2012). An operational ocean forecast systemincorporating NEMO and SST data assimilation forthe tidally driven European North-West shelf. *Journal of Operational Oceanography*, *5*, 3–17. doi: 10.1080/1755876X.2012.11020128

O'Dea, E., Furner, R., Wakelin, S., Siddorn, J., While, J., Sykes, P., ... Hewitt, H. (2017). The CO5 configuration of the 7 km Atlantic Margin Model:large-scale biases and sensitivity to forcing, physics optionsand vertical resolution. *Geoscientific Model Development*, *10*, 2947–2969. doi: 10.5194/gmd-10-2947-2017

Opdal, A., Lindemann, C., & Aksnes, D. (2019, September). Centennial decline in North Sea water clarity causes strong delay in phytoplankton bloom timing. *Global Change Biology*, *25*(11), 3946–3953. doi: 10.1111/gcb.14810

Orlanski, I. (1976). A simple boundary condition for unbounded hyperbolic flows. *Journal of Computational Physics*, *21*, 251–269. doi: 10.1016/0021-9991(76)90023-1

Röttgers, R., Heymann, K., & Krasemann, H. (2014). Suspended matter concentrations in coastal waters: Methodological improvements to quantify individual measurement uncertainty. *Estuarine, Coastal and Shelf Science*, *151*, 148–155. doi: 10.1016/j.ecss.2014.10.010

Sanford, T., & Lien, R.-C. (1999). Turbulent properties in a homogeneous tidal bottom boundary layer. *Journal of Geophysical Research: Oceans*, *104*(C1), 1245-1257. doi: https://doi.org/10.1029/1998JC900068

Saulquin, B., Gohin, F., & Garrello, R. (2011). Regional objective analysis for merging high-resolution meris, modis/aqua, and seawifs chlorophyll- a data from 1998 to 2008 on the european atlantic shelf. *IEEE Transactions on Geoscience and Remote Sensing*, *49*(1), 143–154. doi: 10.1109/TGRS.2010.2052813.

Schartau, M., Riethmüller, R., Flöser, G., van Beusekom, J., Krasemann, H., Hofmeister, R., & Wirtz, K. (2019). On the separation between inorganic and organic fractions of suspended matter in a marine coastal environment. *Progress in Oceanography*, *171*, 231–250. doi: 10.1016/j.pocean.2018.12.011

Song, Y., & Haidvogel, D. (1994). A semi-implicit ocean circulation model using a generalized topography-following coordinate system. *Journal of Computational Physics*, *115*(1), 228–244. doi: 10.1006/jcph.1994.1189

Stanev, E., Dobrynin, M., Pleskachevsky, A., Grayek, S., & Günther, H. (2009, April). Bed shear stress in the southern North Sea as an important driver for suspended sediment dynamics. *Ocean Dynamics*, *59*(2), 183–194. doi: 10.1007/s10236-008-0171-4

Sykes, P., & Barciela, R. (2012, 4). Assessment and development of a sediment model within an operational system. *Journal of Geophysical Research: Oceans*, *117*, 4036–. doi: 10.1029/2011JC007420

Thewes, D., Stanev, E., & Zielinski, O. (2020). Sensitivity of a 3D Shelf Sea Ecosystem Model to Parameterizations of the Underwater Light Field. *Frontiers in Marine Science*, 816. doi: 10.3389/fmars.2019.00816

Twardowski, M., Boss, E., Macdonald, J., Pegau, W., Barnard, A., & Zaneveld, J. (2001). A model for estimating bulk refractive index from the optical backscattering ratio and the implications for understanding particle composition in case i and case ii waters. *Journal of Geophysical Research: Oceans*, *106*(C7), 14129-14142. Retrieved from `https://agupubs.onlinelibrary.wiley.com/doi/abs/10.1029/`

2000JC000404 doi: https://doi.org/10.1029/2000JC000404

Umlauf, L., & Burchard, H. (2003, March). A generic length-scale equation for geophysical turbulence models. *Journal of Marine Research*, *61*(2), 235–265. doi: 10.1357/002224003322005087

van der Molen, J., Ruardij, P., & Greenwood, N. (2017). A 3D SPM model for biogeochemical modelling, with application to the northwest European continental shelf. *Journal of Sea Research*, *127*, 63–81. doi: 10.1016/j.seares.2016.12.003

Vanhellemont, Q., & Ruddick, K. (2021). Atmospheric correction of sentinel-3/olci data for mapping of suspended particulate matter and chlorophyll-a concentration in belgian turbid coastal waters. *Remote Sensing of Environment*, *256*. doi: 10.1016/j.rse.2021.112284

Wakelin, S., Artioli, Y., Butenschön, M., Allen, I., & Holt, J. (2015, 07). Modelling the combined impacts of climate change and direct anthropogenic drivers on the ecosystem of the northwest european continental shelf. *Journal of Marine Systems*, *152*. doi: 10.1016/j.jmarsys.2015.07.006

Wakelin, S., Holt, J., Blackford, J., Allen, J., Butenschön, M., & Artioli, Y. (2012). Modeling the carbon fluxes of the northwest european continental shelf: Validation and budgets. *Journal of Geophysical Research: Oceans*, *117*(C5). Retrieved from https://agupubs.onlinelibrary.wiley.com/doi/abs/10.1029/2011JC007402 doi: 10.1029/2011JC007402

Warner, J., Sherwood, C., Arango, H., & Signell, R. (2005). Performance of four Turbulence Closure Methods Implemented using a Generic Length Scale Method. *Ocean Modelling*, *8*(1-2), 81–113. doi: 10.1016/j.ocemod.2003.12.003

Wilson, R., & Heath, M. (2019). Increasing turbidity in the North Sea during the 20th century due to changing wave climate . *Ocean Sciences*, *15*. doi: 10.5194/os-15-1615-2019

Wiltshire, K., Malzahn, A., Wirtz, K., Greve, W., Janish, S., Mangelsdorf, P., ... Boersma, M. (2008). Resilience of North Sea phytoplankton spring bloom dynamics: An analysis of long-term data at Helgoland Roads. *Limnology and Oceanography*, *53*(4), 1294–1302. doi: 10.4319/lo.2008.53.4.1294

Wollschläger, J., Tietjen, B., Voß, D., & Zielinski, O. (2020). *Frontiers in Marine Science*, *7*, 512. Retrieved from https://www.frontiersin.org/article/10.3389/fmars.2020.00512 doi: 10.3389/fmars.2020.00512

Xiu, P., & Chai, F. (2011). Modeled biogeochemical responses to mesoscale eddies in the South China Sea. *Journal of Geophysical Research*, *116*. doi: 10.1029/2010JC006800

Xiu, P., & Chai, F. (2014, March). Connections between physical, optical and biogeochemical processes in the Pacific Ocean. *Progress in Oceanography*, *122*, 30–53. doi: 10.1016/j.pocean.2013.11.008